Forecasting Research Division
Technical Report No. 64

DIAGNOSING SYSTEMATIC ERRORS IN THE UNIFIED MODEL I - THERMAL BUDGET

by
S.F. Milton

September 1993

1. INTRODUCTION

All current Numerical Weather Prediction (NWP) and climate models show growth of systematic errors (SE) as they are integrated from their initial conditions. This "Climate Drift" is the approach of the model towards its own climate equilibrium consistent with its representation of dynamical and physical atmospheric processes. Diagnosing the ***source*** of model SE growth is a complex problem owing to the coupled, non-linear, nature of the equations governing atmospheric motion. For example an error in the temperature field can arise directly from inaccurate representation of heat fluxes or diabatic heating in the model, or indirectly via errors in the momentum budget to which the temperature field adjusts to maintain thermal wind balance. The problem is further compounded by the fact that errors may propagate over large distances in relatively short time periods on the order of a few days (Klinker, 1990), making it difficult to identify locally forced errors from those remotely forced.

A recent technique for diagnosing the source of model SE, developed by Klinker and Sardesmukh (1987;1992) at ECMWF, attempts to address some of the above problems. The technique involves running a large number of very short range forecasts of one or two timesteps and examining the time-mean thermal and momentum budgets in terms of the contributions from each model routine. Klinker and Sardesmukh showed that errors in the "initial tendencies" bore a strong resemblance to the 6hr and medium-range forecast errors, and hence could be used to assess the relative contribution of each model routine to the SE. The technique has a number of potential advantages

(i) Errors due to thermal and momentum forcing have no time to interact.
(ii) Local errors are emphasised, not remote forcing.
(iii) The integrations are inexpensive.

Given the relative success of the technique at ECMWF and its application at other operational forecast centres such as NMC (Kanamitsu and Saha, 1992), it was decided to apply a similar approach to the global Unified Model (UM). This paper concentrates upon the SE in temperature which manifests itself as a global cooling of the troposphere in both short-range forecasts and climate simulations. Section 2 outlines the details of the diagnostic technique, version of the UM used and the integrations carried out. The SE in the operational version of the UM run during December 1992 is described in section 3. Section 4 contains the bulk of the results from the one timestep budgets, and section 5 deals with the sensitivity of the UM thermal budget to operational changes in moisture diffusion in the model. The time evolution of the thermal budget between T+00 and T+72 is discussed in section 6.

Conclusions and proposals for future work are given in section 7.

2. MODEL DESCRIPTION AND TECHNIQUES.

The thermal budget in the model can be written in the form of a time-mean temperature tendency equation as

$$\left(\frac{\overline{\partial T}}{\partial t}\right)_{MODEL} = \left(\frac{\overline{\partial T}}{\partial t}\right)_{DYN} + \left(\frac{\overline{\partial T}}{\partial t}\right)_{PARAM} \qquad (1)$$

which states that the total time-mean temperature tendency is the sum of the temperature tendency from the dynamics scheme, commonly referred to as the adiabatic component, and those from the model's parametrization schemes, referred to as the diabatic component. The overbar indicates a time averaging operator. Similar equations can be written for other model prognostic variables such as moisture and winds. For a model in climate equilibrium one expects the time-mean adiabatic and diabatic components to be of equal magnitude and opposite sign (Boville, 1985). However in the initial stages of a model integration when significant SE growth is occurring the total tendency in equation 1 should reflect the systematic tendency of the model temperature to change with time as the model drifts towards its own climate. Equation 1 can be rewritten as

$$\left(\frac{\overline{\partial T}}{\partial t}\right)_{MODEL} = \left(\frac{\overline{\partial T}}{\partial t}\right)_{ANALYSIS} + \overline{E} \qquad (2)$$

where $\overline{E}$ is a measure of the systematic error in the initial tendencies with respect to the analysed atmospheric state, the so called systematic "initial tendency error", defined as the mean model tendency minus the analysed trend over the period of the time mean. The analysed trend is generally small for time means but can easily be calculated.

In forecasts of one or two timesteps contributions to E may come from the following sources

(i) Data assimilation errors
(ii) Observational errors
(iii) Model error.

The first two represent *systematic* deficiencies in the specification of the initial state. For example if the model were a perfect representation of the atmosphere and we presented it with an initial state

which was systematically biased with respect to the *true* atmospheric state, then we would see a trend in the model temperature as the model moved away from the analysed state towards the *true* climate equilibrium state. Similarly an imperfect model presented with the *true* atmospheric state would show a trend in temperature as the model moved towards its own climate equilibrium state. The real situation is a combination of these two factors and differentiating between errors to the input to the model and errors in model formulation is difficult. One of the main aims is to demonstrate that the initial tendencies from short-range forecasts bear a strong resemblance to the SE at later forecast ranges. The systematic component to the error budget at these longer forecast ranges is dominated by deficiencies in model formulation rather than analysis errors.

Within the UM system the tendencies due to each model routine are calculated from temperatures output after the routine. This is straightforward for most routines but is more complicated for the dynamics and large-scale cloud due to the use of cloud conserved thermodynamic variables (see Appendix A for discussion). It should be borne in mind that this technique only considers the processes which directly impact upon the thermal budget and does not take account the modifying influence on the temperature field which may arise from SE growth in the momentum budget due to parametrizations such as gravity wave drag.

In order to carry out the budget calculations the UM was integrated from the 4 operational analyses (00Z, 06Z, 12Z, and 18Z) for the period 00Z 1 December 1992 - 00Z 1 January 1993, a total of 125 integrations. Each integration was two timesteps in length and the temperature increments from each model routine were calculated as increments to the total temperature change between timestep 1 and 2. All increments were then averaged over the 125 integrations to filter out any random components.

Version 2.7 of the UM was run at the operational resolution of 217 * 288 latitude/longitude points and 19 vertical hybrid levels. All parametrizations were as used operationally during December 1992. Differences in parametrization between the operational and climate versions of the UM are given in appendix B. Use of the operatinal version of the UM allows direct comparison between the SE from the operational runs at various forecast ranges (T+24 - T+120) and the initial tendency errors ($\overline{E}$) calculated from the 2 timestep integrations.

One difference from the operational configuration is that the 2 timestep integrations are run from T+00 analyses whereas in the operational model the assimilation increments are still applied with reducing weights for a further 4 hours after T+00.

It must be noted that since carrying out the runs for December 1992 an error in the gravity wave drag scheme has been corrected. This has led to a reduction of the cold bias in the Northern Hemisphere (NH) , but the overall structure of the cooling decribed in this paper has not changed.

3. SYSTEMATIC ERRORS IN OPERATIONAL UNIFIED MODEL FORECASTS.

The zonally-averaged and time-mean temperature error formed as the 30-day mean difference between T+72 forecasts and their T+00 verifying analyses (Fig. 1) shows the model tendency to cool almost everywhere. Maxima of between -1.5 K and -2.0 K can be seen at the tropical tropopause and in the extratropical troposphere at 30°S-60°S with a smaller cooling at 20°N-50°N. In the tropics there is a tendency to warm below the tropopause and warming also occurs at the polar regions (note: calculations are carried out on standard pressure levels and care must be taken where extrapolation occurs below orography, such as over Antarctica). In the Northern Hemisphere (NH) there is a cooling of between -1.0 K and -1.5 K at 1000mb between 50°N and the pole. Similar error patterns occur in the T+24 and T+48 SE but with reduced magnitude.

The geographical distribution of the temperature SE for December 1992 at 850mb and 250mb are shown in fig. 2. All fields have been interpolated to the climate resolution of 73 x 96 latitude/longitude points prior to plotting, which smooths the fields but retains the large-scale features of interest. At 850mb (fig. 2(a)) the cooling in the (NH) is confined mainly to the oceanic sectors in the regions characterised by the stormtracks, with maxima over the south eastern U.S and south east China stretching northeastwards acoss the ocean basins. These are areas where the fluxes of sensible and latent heat are maximum and the net heat flux is from ocean to atmosphere as the cold continental air moves over the warm ocean currents of the Gulf stream and Kuroshio current. The land areas show a tendency to warm, noteably over Asia, NW Canada, and central Africa. In the Southern Hemisphere (SH) the cooling maxima are larger in magnitude and are linked to the subtropical high pressure systems (see Fig. 3(c)). Another interesting feature is the warming which occurs off the western coasts of the continents of South America, North America and Africa. These are regions of the cold ocean currents (Peruvian, Californian, and Benguela) where the net heat flux is from atmosphere to ocean and persistent areas of stratocumulus and stratus clouds are formed. Other regions of warming can be seen in the Amazon, Indian ocean and Indonesia where convective activity is a maximum, and along the edge of Antarctica. The patterns of cooling and warming are similar at 250mb in the extratropics but cooling dominates the tropical regions. The tropospheric cooling is a robust error which is present in all seasons. It is also a feature of a number of NWP and climate models (Bourke et. al, 1991; Boer et. al., 1991).

4. THERMAL BUDGET FROM TWO TIMESTEP INTEGRATIONS.

Having identified the structure of the UM SE in temperature we now consider the thermal budget in more detail as calculated from the two timestep integrations.

(i) Zonally averaged thermal budget.

The first aim is to demonstrate that the initial tendency error ($\overline{E}$) in model temperature reflects the model SE described in the previous section. The zonally averaged model total tendency (LHS of equation 2) calculated on model levels is shown in figure 3(a). The abscissa is the model eta values which is approximately equal to pressure divided by 1000mb. This total tendency term is generally 5-10 times larger than the analysed trend for December 1992 (Fig. 4) and hence for the remainder of the paper we take the approximate form of equation 2 in which the model total tendency is equal to the "initial tendency error".

$$\left(\overline{\frac{\partial T}{\partial t}}\right)_{MODEL} \simeq \overline{E} \qquad (3)$$

The total tendency shows most of the features seen in the zonally averaged temperature error (Fig. 1). There are cooling maxima in the extratropics in both hemispheres, cooling at the tropical tropopause, and warming in the tropics and over both poles (n.b. :- the warming over Antarctica is not an artefact of interpolation as all calculations are performed on model eta levels). The tendencies even reflect some of the finer detail seen in the SE, such as the -0.4 K/day contour reaching the surface in the SH but not the NH. Large cooling tendencies can also be seen at the lower boundary in the NH from 20°N-80°N. A similar cooling is apparent in the T+72 SE but is confined to a smaller latitude range and of smaller magnitude. Large tendencies of both sign can be seen at the upper boundary. However this is not resolved in the T+72 SE plot which only goes to 30mb compared to ~ 5mb for the models top level. One feature of the tendencies which is not consistent with the SE is the 1 K/day warming of the SH polar stratosphere where a cooling of 1 K is a feature of the SE. This is partially accounted for by the analysed trend (Fig. 4) which shows a warming of 0.6 K/day in this region and should be subtracted from the total tendency in order to give us the true value of E.

It should be noted that the T+72 SE and the temperature tendency are of the same magnitude, despite the fact that the tendency is scaled to K/day and therefore representative of a T+24 error. One cannot expect quantitative agreement between the tendency and SE as the SE growth may not be

linear. However the excellent qualitative agreement between the tendency and SE allows us to investigate the contributions of individual model routines to the "errors" in the thermal budget.

Consider the zonally averaged version of equation 1. We can split the total temperature tendency into contributions from the model dynamics (adiabatic component) and parametrization schemes (diabatic component). Following Klinker and Sardesmukh (1992) the sign of the adiabatic component has been reversed to allow easy comparison with the diabatic terms. This is shown in Fig. 3(b) and represents the diabatic heating that the model parametrizations need to provide in order to exactly balance the adiabatic terms of the model dynamics. The diabatic heating supplied by the model is the sum of contributions from the parametrizations of radiation, boundary layer, large-scale cloud, large-scale precipitation and convection and is shown in figure 3(c). The heating rates in Fig 3(c) minus those in Fig. 3(b) give the total temperature tendency (Fig 3(a)).

For the dynamics there is a cooling in the tropics (allowing for the change of sign) from ascent in the Hadley circulation and a shallower region of cooling up to 400mb in the extratropics associated mainly with the horizontal and and vertical transport of heat by the eddies in the stormtrack regions. Warming occurs in the subtropics where there is large scale descent, with a stronger maxima in the NH compared to the SH. The parametrized diabatic heating (Fig. 3(b)) agrees well with the adiabatic cooling in the tropics, hence the small warming tendencies. It must be borne in mind that any lack of data to constrain the model means that the adiabatic vertical motion in the model may be strongly influenced by the convective scheme via the assimilation cycle, and for this reason differences in dynamical and parametrized forcing may be small. In the subtropics at 20°N and 25°S there is a parametrized cooling, due mainly to radiative processes, which is not balanced by the adiabatic warming due to descent in the Hadley cell and leads to an overall cooling tendency (Fig. 3(a)). In the extratropics the parametrized diabatic heating is insufficient to balance the adiabatic cooling. Indeed in the NH the parametrized diabatic heating is negative everywhere (this is only true in the zonal average), and in the SH the main area of parametrized diabatic heating is located at 60°S at 600mb compared with the adiabatic cooling maxima which occurs at 48°S and 600mb. This shift accounts for the cooling-warming dipole between 40°S-80°S seen in both the temperature tendency and the T+72 SE. The parametrized diabatic heating also has a band of cooling at the tropopause from pole-to-pole which has no counterpart in the adiabatic terms. The difference between the two shows up clearly as the systematic cooling at the tropopause (Fig. 3(a) and Fig. 1).

The planetary-scale diabatic heating distribution is poorly observed and current estimates calculated

using both radiosonde data and model analyses show large uncertainties (Holopainen, 1987). This makes it difficult to validate whether the diabatic heating estimated from the model dynamics (adiabatic component) is more accurate than that produced by the model parametrizations. In order to assess the uncertainties in our estimates of diabatic heating from December 1992 we have compared them with those calculated routinely from ECMWF operational analyses at Reading University (Hoskins et al., 1989). The diabatic heating ic calculated as a residual in the time-averaged thermodynamic energy equation using circulation data generated from the operational ECMWF analyses,

$$\overline{Q} = \frac{\partial \overline{T}}{\partial t} + \overline{\underline{v}}.\underline{\nabla}\overline{T} + \left(\frac{p}{p_o}\right)^{\frac{R}{c_p}} \overline{\omega}\frac{\partial \overline{\theta}}{\partial t} + \left(\frac{p}{p_o}\right)^{\frac{R}{c_p}} \left[\underline{\nabla}.\overline{\underline{v}'\theta'} + \frac{\partial(\overline{\omega'\theta'})}{\partial p}\right] \qquad (4)$$

where Q is the diabatic heating, an overbar is a time mean and primed quantities are deviations from the time mean. The first term on the RHS is the analysed tendency over the month and the remaining terms the horizontal and vertical transports due to the mean flow and the eddies, the so called "dynamical" terms. This calculation and our adiabatic component (with the sign reversed) are effectively the same calculation (allowing for the small contribution from the analysed trend in the ECMWF estimate).

Contrasting the ECMWF zonally averaged diabatic heating for the first and second half months of December 1992 (Fig. 5 (a) and (b)) with our calculations, we note that the overall distributions are very similar. In the extratropical regions there is a warming in both hemispheres up to 500mb as seen in our adiabatic component. However close inspection shows that the warming in this region is typically between 0.2 K/day and 0.4 K/day, with a maximum value between 0.4 K/day and 0.6 K/day in the SH during the second half month. These estimates lie between our adiabatic component and our parametrized diabatic heating and highlight the uncertainty in estimating the diabatic heating using different models. A further estimate of diabatic heating calculated from FGGE III data by Fortelius and Holopainen (1992) using equation 4 (Fig 5(c)) shows similar distributions to our results and to those calculated from ECMWF analyses. In mid-latitudes their estimate is greater than our parametrized terms and close to our adiabatic terms, but the tropical diabatic heating appears to be less than both our adiabatic/parametrized terms and the ECMWF calculation. Other model estimates of diabatic heating rates include those calculated from the ECMWF model adiabatic terms during January 1987 (Klinker and Sardesmukh, 1987). These are close to the estimates from our adiabatic terms in the UM. Despite the uncertatinties between the various estimates of diabatic heating the evidence from these studies suggests that the parametrized diabatic heating in the UM is underdone

in the extratropical regions during the early stages of forecasts.

It is worth pointing out that the problem may not actually lie with the formulation of any parametrization itself, but rather with the inputs to the parametrization scheme. For example Klinker and Sardesmukh (1987) showed a strong sensitivity of parametrized diabatic heating in the stormtrack regions to the specification of the initial moisture field. This point is further addressed in section 5 and section 6.

The zonal cross sections of the parametrized heating increments due to each model routine are shown in figures 6 to 8. Detailed discussion of the balance is given in the next section and a brief outline of each contribution is given here. The total radiative heating increment (Fig. 6(c)) clearly shows a large cooling at the tropopause level from north to south pole, which is evident in the total parametrized heating (Fig. 3(c)) and accounts for the cooling tendencies (Fig 3(a)) and the SE in temperature (Fig. 1). Similar excessive radiative cooling at the tropopause was found in the ECMWF model by Klinker (1992 - see his Fig. 4(c) and 5(b)). It should be noted that the radiative cooling is even larger in the UM if the ECMWF LW transmissivities are not used (Rawlins, 1992). The turbulent mixing due to the boundary layer scheme is dominated by the contributions at the lowest model levels (Fig 7(a) - note the expanded vertical scale) and is in approximate balance with the large negative tendencies in the convection scheme (Fig. 7(b)). The convective heating is confined mainly to the tropics, where it balances the adiabatic and radiative cooling, and also to the extratropical boundary layer. There appears to be little convective heating above the boundary layer in the extratropics, at least in the zonal average. Most of the extratropical heating comes from the latent heat release due to the formation of large-scale cloud (Fig. 8(a)). The layer and convective cloud distributions from the first timestep are shown in Fig. 8(b) and 8(c) respectively. Finally the large-scale precipitation scheme contributes a relatively large cooling below 600mb in the extratropics due to the evaporation of precipitation. This is of the order of -1 K/day near the surface.

(ii) Vertical profiles of the heating rates

To gain a clearer picture of the relative contributions of each model routine to the parametrized diabatic heating, vertical profiles of the zonally averaged heating rates have been plotted for selected latitudes.

(a) *NH mid-latitudes, 40°N*

This latitude is chosen as it is the location of the largest temperature SE (Fig. 1). The profile of the

total tendency (Fig. 9(a)) can be partitioned into 3 distinct regions. The lowest model level where there is a large cooling tendency of -3.5 K/day, the remainder of the boundary layer and troposphere between levels 2 (975mb) and 14 (150 mb) where there is a uniform cooling of the order -0.5 to -1.0 K/day and finally the stratosphere (levels 15 to 19) where the cooling again increases to -3.5 K/day in the top model level.

If the model were in thermal balance then the parametrized heating profile and the dynamical heating profile (with sign reversed) should be coincident. This is clearly not the case (Fig. 9(b)) with the parametrized heating typically 1 K/day cooler, although for levels 3-12 the parametrized and dynamical heating rates do show similar vertical variation. The only point where the parametrized heating warms the atmosphere is at levels 2 and 3 in the boundary layer, whereas the dynamics requires a warming up to at least level 9 ($\sim$422mb) in order for thermal balance to be achieved. In level 1 and level 19 both parametrizations and dynamics act in the same sense, cooling the model atmosphere, hence the large overall cooling tendencies in Fig 9(a). In fact at level 1 the parametrized heating rate would need to change by +3 K/day in order to balance the dynamical contribution, whilst at level 2 they are in balance. Of course it cannot be ruled out that such large tendencies in top and bottom levels are not due to some rapid adjustment processes which damps down after several timesteps. However there is evidence of a surface cooling in the model SE in the NH (Fig. 1).

The individual contributions to the parametrized heating are shown in Figure 9(c). For the boundary layer (levels 1-5) the LW radiation and large scale precipitation provide almost constant cooling which combined comes to -3 K/day. This is partially balanced by the constant warming of +0.5 K/day due to SW radiation. The convective and boundary layer schemes show more vertical variation in heating. In the lowest model level they are almost equal and opposite and very large in magnitude ($\sim$ 20 K/day). This suggests that the large heating of the lowest layer by the boundary layer scheme is effectively removed from this layer by the convection scheme. Above level 1 the convection scheme warms the boundary layer with a maxima at level 3 and very little heating in the free troposphere. The boundary layer scheme operates mainly in the bottom two levels with small heating rates at levels 3-5. Further runs have been carried out for the North Atlantic sector to look at individual point profiles rather than zonal averages. Similar results are found with very little convective heating occurring above the boundary layer in the stormtracks. From levels 5-10 the latent heat release due to the large-scale cloud scheme provides the main positive contribution to the total temperature tendency, but is insufficient to balance the radiative and adiabatic cooling. In the stratosphere the balance involves only radiative and dynamical forcing, with imbalance between the

warming due to SW and cooling of the LW and dynamics schemes.

Assuming that the extratropical parametrized heating is deficient, it remains a difficult task to determine which parametrization(s) is(are) in error. Possible candidates for the cooling of the troposphere in the extratropical stormtracks are,

(i) Insufficient condensational heating from the large-scale cloud scheme.
(ii) A lack of convective heating above the boundary layer.
(iii) Excessive radiative cooling.
(iv) Too much evaporative cooling from the precipitaion scheme.
(v) A missing physical process - Slantwise convection ?

The LW radiative term of -1.5 K/day does not seem excessive compared to other models and certainly cannot account for a difference as large as 1 K/day between parametrized and dynamical terms. More likely candidates are the moist processes of convection and large-scale cloud. Their sensitivity to the moisture distribution is discussed further in sections 5 and 6. A further possibility is that an important physical process is not represented in the model. It has been suggested that slantwise convection may be important in the mid-latitude thermal budget.

In the boundary layer their is a complex interaction between the convection scheme and boundary layer turbulent mixing. It is unclear whether the extratropical convective heating profiles being largely confined to the boundary layer is realistic. It is also questionable whether the boundary layer scheme should confine most of its heating to the lowest model levels. Recent experiments with alternative formulations of the boundary layer scheme using a non-local mixing criterion and with the convective scheme including downdraughts (Smith, 1993), show a reduction in the large tendencies in the lowest model level and more turbulent mixing in levels 3 and 4 due to boundary layer scheme. More work is needed to understand these interactions between the boundary layer and convection schemes. Finally, it is also possible that the cooling due to evaporation of dynamical precipitation may be excessive in these lowest model layers.

(b) *Tropics, 5°S*

The thermal balance in the Tropics is an improvement over that in mid-latitudes, with parametrizations and dynamics in approximate balance up to level 9 (Figs 10(a) and (b)). In the

troposphere most of the warming is provided by convection and SW radiation which are balanced by the LW radiative and adiabatic (dynamical) cooling. Above level 9 there is a net cooling of order -1 K/day in the total tendency. This is coincident with a peak in the radiative forcing which is coincident with the high layer cloud present at the tropical tropopause (Fig. 8(b)), and may suggests that the radiative cooling is too intense.

(c) *SH mid latitudes, 42°S*

Overall the degree of balance at this latitude is similar to 40°N with parametrized heating rates consistently less than dynamical heating rates throughout the troposphere (Fig 11). One noteable difference is the tendency in the lowest model level which is much less than its counterpart in the NH. This may suggest that the large cooling tendencies in the NH lowest level are linked to the land. The contributions from boundary layer turbulent mixing and convection in the lowest model layer are much smaller than in the NH or tropics (Fig. 11(c)). A further difference is the large spike in the SW and LW radiative increments in model level 3. This is associated with the large cloud amounts in the SH boundary layer at these latitudes (Fig. 8(a)). This problem of excessive low cloud over the summer oceans is a known deficiency of the UM. G.White (personal communication) at NMC has noted that in the assimilation cycles the UKMO surface energy budget is very different to that of ECMWF and NMC in the SH mid-latitudes in December, with the UM net SW radiation at the surface some 70 W/m^2 less than ECMWF/NMC due to this low cloud and the net surface LW less by 35 W/m^2 presumably due to low cloud providing a larger downward LW flux (see Milton, 1993).

(iii) Geographical heating distributions.

As with the zonally averaged results we would like to demonstrate that the geographical distribution of the total tendency in model temperature over the the first few timesteps of integration resembles the known systematic error at later forecast ranges. Comparison of the total tendency at model level 4 ($\eta = 0.867 \sim$ 850mb) (Fig 12(a)) calculated from the one timestep tendencies averaged over the 125 integrations, and the T+72 SE in temperature at 850 mb (Fig. 2(a)) reveals several remarkable similarities. These include the cooling in the NH stormtrack regions, cooling in the SH oceans coincident with the subtropical high pressure systems, warming over the central African, Amazon and Indonesian regions. Warming also occurs off the western coasts of South America, Africa and California in regions characterised by persistent stratocumulus/stratus cloud.

The parametrized diabatic heating (Fig. 12(c)) and the negative of the dynamical heating (Fig 12(b)) generally have very similar geographical distributions and any systematic differences are subtle. The

parametrized heating in the NH stormtracks is less in magnitude than the adiabatic cooling with the largest imbalance occurring over Japan. The warming in the Indonesian region arises from a parametrized heating rate in excess of 4 K/day compared to an adiabatic cooling of only -2 K/day to -4 K/day. Over the Sahel and Amazon regions the parametrizations provide a warming but the adiabatic terms also warm, leading to the overall warming tendencies in Figure 12(a). The warming over the western continents of South America and Africa is a well known problem in the UM and other models and arises from the models inability to maintain the correct distribution of stratocumulus cloud near the coasts. This can be seen in the parametrized terms where the cooling near the coasts is less than in mid-ocean. In the SH the adiabatic terms suggest that there should be large areas of diabatic heating over much of the southern oceans between 40°S and 65°S with maxima to the west of South America and stretching from South Africa to Australia. The parametrized heating has maxima in the correct longitudes but they are confined to a narrower latitude band and don't stretch far enough equatorward. This behaviour was noted in the zonally-averaged budget and leads to the warming tendency along the edge of Antarctica.

The total radiative contribution to the parametrized heating cools everywhere (Fig. 13(c)) and is largest over the subtropical oceans associated with the persistent low cloud. The impact of too little stratocumulus cloud is again evident with smaller values of radiative cooling near the western continental coasts. It is interesting that the radiative cooling is at its smallest ($>$-1K/day) in the NH stormtrack regions where the total temperature tendency (Fig. 12(a)) and the temperature SE (Fig 2(a)) are largest. The heating/cooling rates due to radiation in a given layer are obviously very sensitive to the presence of cloud in that layer. It may be more representative to consider vertical integrals of radiative increments over a number of vertical levels (e.g. the boundary layer) rather than just one layer. The subtropical maxima in radiative cooling are largely balanced by the warming increments from the boundary layer scheme (Fig 14(a)). As noted in the zonally averaged results the largest contribution from turbulent boundary layer mixing occurred in levels 1 and 2 and was virtually negligible in the remaining boundary layer levels. These subtropical maxima in level 4 arise from the latent heat release due to the formation of layer cloud in the call to the large-scale cloud scheme from within the boundary layer scheme. At level 4 the major positive contribution to the parametrized diabatic heating is from convection, which occurs in the ITCZ, tropical convective regions of Indonesia, Amazon and Africa, and in the NH stormtracks. The warming in the total tendency over the tropical land areas may indicate that the convective heating is too intense in these regions. The large scale precipitation scheme cools in the extratropics due to the evaporation of precipitation (Fig. 14(c)), and its largest values are in the NH stormtracks where they exceed -2

K/day. These values may be excessive and their reduction could lead to an increase in the parametrized diabatic heating rate. Finally the latent heat release due to the large-scale cloud scheme (Fig. 14(d)) warms at 60°S and also in the NH stormtracks where it is generally smaller in magnitude than the convective heating. Higher in the atmosphere at around 700mb it is the cloud scheme which provides the largest warming (Fig. 9). The cloud scheme also has maxima over orography such as the Rockies and Andes. This may be a problem with the horizontal diffusion of moisture along the model vertical coordinate surfaces.

5. SENSITIVITY OF THE THERMAL BUDGET TO MOISTURE DIFFUSION.

A recent operational change was introduced into the global UM which changed the order of moisture diffusion from ∇^2 to ∇^4. This change was implemented as it reduced the UM moist bias. During a parallel trial held in February 1993 the model was run through a complete analysis/forecast cycle with both versions of moisture diffusion. The analyses generated from both analysis/forecast cycles were used to perform a number of two timestep integrations. This section deals with the results from these integrations highlighting the impact of the changes to moisture diffusion on the UM thermal budget.

The total temperature tendency for ∇^2 diffusion (Fig. 15(a)) shows the familiar patterns discussed in earlier sections. The introduction of ∇^4 diffusion (Fig. 15(b)) has a small ($\sim$ +0.2 K/day) but beneficial impact upon the residual cooling at 35°N and 35°S between 500mb and 200mb (Fig. 15(c)). The tropical belt also warms by a similar amount, but this acts to increase the warming tendency at 400mb (Fig. 15(b)) noted in the SE (Fig. 1). The change in the parametrized diabatic heating (Fig 16(c)) accounts for a large proportion of the change in the total tendency. However it is larger in magnitude than the change in the total tendency implying a compensating change in the adiabatic (dynamical) component of the balance. This can be seen in Figure 17(c) with bands of cooling due to increases in large scale ascent at 30°N, 5°N, 5°S and 15°S with increased warming between. This result is important as it suggests that we should only apply the one-timestep technique to analyses and forecasts which use the same model, otherwise the initial tendencies may be masked by adjustments to the different models used in assimilation and forecast, which is a drawback if one wants to look at sensitivity to changes in model parametrizations. The main contributions to the increase in parametrized diabatic heating are from increased convective heating (Fig. 18(c)) of up to +0.5 K/day in the tropics, and from the large-scale cloud scheme (Fig. 19(c)) which increases the warming on the equatorward side of the stormtrack diabatic heating maxima.

In general the changes to moisture diffusion have a beneficial impact on the systematic cooling in the

extratropics, and are entirely beneficial in reducing the UM moist bias (not shown). However they may have enhanced the convective heating and hence the slight warm bias in the tropical atmosphere. The use of these detailed diagnostics gives a better physical understanding of the processes responsible for the changes to temperature upon changing the order of moisture diffusion. They also highlight the sensitivity of the moist parametrizations of convection and large scale cloud to changes in the specification of the initial moisture field.

6. TIME EVOLUTION OF THE THERMAL BUDGET.

Given that the global UM is not in thermal balance in the initial stages of a forecast, it is of interest to determine how the model finally achieves thermal equilibrium. To investigate the time evolution of the thermal budget a number of two-timestep integrations have been run from dumps of the operational model at T+00 and T+72 for data times 00Z and 12Z. A total of 22 integrations were run from each of the model dumps during the first half of July 1993 and the thermal budget determined as in earlier sections. The operational version of the UM was used (version 3.1), which includes the change from ∇^2 to ∇^4 moisture diffusion and the correction to the gravity wave drag scheme implemented in March 1993.

The total tendency determined from T+00 (Fig. 20(a)) is similar in most respects to that from the December integrations (Fig 3(c)) with cooling in mid-latitudes and at the tropical tropopause and warming in the tropics. The warming tendency in the tropics is larger in July. It is not known whether this is a seasonal effect, a consequence of the change to moisture diffusion, or a function of the fact that we have only 22 integrations in the July budget compared to 125 in the December budget. As before we note that there is an imbalance between parametrized diabatic heating (Fig 20(c)) and the adiabatic cooling (Fig 20(b)) in the stormtracks. The parametrized diabatic heating in the tropics has a maxima of +6 K/day compared to -5 K/day from the dynamics, hence the warming tendency. In addition the cooling in the subtropics due to the parametrizations is larger than the compensating adiabatic warming due to the Hadley circulation.

At T+72 the total tendencies have reduced dramatically (Fig. 21(a)) in both the tropics and extratropics consistent with the models approach to thermal equilibrium. Careful inspection of the dynamical component of heating (Fig. 21(b)) show relatively small differences to T+00, with a slight decrease in the dynamical cooling at 10°N and 400mb due to a reduction in large scale ascent, but similar cooling rates in the stormtrack regions. The parametrized diabatic heating (Fig. 21(c)) has increased in the stormtrack areas giving better balance with the adiabatic cooling, although generally

the parametrized heating is still less in magnitude. In the tropics the parametrized heating has decreased from +6 K/day to between +4.5 to +5 K/day which gives good balance with the adiabatic cooling of between -4.5 to -5 K/day at T+72. In isolation the detailed knowledge of thermodynamic balance at the point the model has achieved equilibrium provides no insight into the source of the model SE, but armed with the thermal budget at T+00 we have a powerful diagnostic tool which highlights the areas of largest sensitivity in the thermal balance during the period of "Climate Drift", and may indicate possible sources of model SE.

The changes in latent heating between T+00 (Fig. 22(a)) and T+72 (Fig 22(b)) due to the formation of large-scale cloud provide the main contribution to the increase in parametrized diabatic heating in the stormtracks. This is accompanied by an increase in the large scale cloud fraction (Fig. 25(a)-(c)) over most of the extratropics. Particularly large are the increases in low cloud over the summer hemisphere. Over the tropics and SH the low cloud in the bottom model levels decreases. There is also an increased cooling from the evaporation of rainfall (not shown) arising from the increase in dynamical precipitation rates. All of the above implies a considerable "spin-up" in the hydrological cycle of the model in the extratropical regions, which is linked to the deficiencies in the extratropical parametrized heating in the initial stages of the forecasts. Changes in convective heating (Fig. 23(c)) show the decrease at 10°N in the tropical maxima noted in the parametrized diabatic heating. However in the extratropics there is an increase in convective heating which is confined to the boundary layer in the SH but penetrates as high as 300mb between 30°N and 60°N, contributing to the increase in parametrized diabatic heating in the NH stormtrack. These increases in convective heating are reflected in a spinup in convective cloud fraction and precipitation (Fig 26(d)). The increase in convective heating between 10°N-20°N and 500-200mb (Fig. 23(c)) is a consequence of a slight northward shift in the tropical heating maxima between T+00 and T+72.

Obviously with the changes in the large scale cloud fraction there are accompanying changes in radiative increments (Fig. 24(a)-(c)). Where there are local increases (decreases) in cloud (Fig. 25(c)) there is a local increase (reduction) in the radiative cooling (Fig. 24(c)) which comes mainly from the LW forcing. This demonstrates the tendency of clouds to cool the atmosphere locally (Slingo and Slingo, 1988). In the NH and the tropics there is also a reduction in radiative cooling in the layers immediately below the increased high cloud which shows up as a warming in the T+72 - T+00 difference field (Fig. 24(c)). This is due to the increased 'greenhouse effect' of the clouds on the layers below. The increases in high cloud act overall to reduce the large gradient in radiative cooling across the tropopause (Fig. 24(a) and 24(b)). The effect of this can also be seen in the total parametrized diabatic heating at T+72 which has a smaller cooling tendency at 400mb in the NH.

For low cloud we note that increases in the NH enhance the radiative cooling and the decreases in the SH reduce the radiative cooling.

Finally, the hydrological balance in the model is shown at T+00 and T+72 (Fig. 26). This confirms the discussion earlier. There is a considerable spin-up in the dynamical and convective rainfall in the extratropics (Fig. 26(c) and 26(d)). There is also a decrease in convective rainfall in the tropics which is consistent with the reduction in convective heating (Fig. 23(c)). The global evaporation rate remains almost constant between T+00 and T+72 (Fig. 26(b)). Even by T+72 their is still an imbalance between global precipitation and evaporation (see global averages).

7. CONCLUSIONS

The aim of this paper has been to investigate the ***source*** of the systematic error (SE) in temperature in the global Unified Model (UM), which manifests itself as a tropospheric cooling. A diagnostic technique has been applied which determines the time-mean thermal budget from a large number of short (2 timestep) integrations. We have shown, following Klinker and Sardesmukh (1992), that the systematic "initial total tendency" in temperature derived from this budget bears a remarkable qualitative resemblance to the model SE at later forecast ranges (T+72), both for the zonally averaged and the local thermal budget. Having demonstrated this link between total tendency and the model SE, we are then able to consider the contribution of individual model parametrizations and model dynamics to the total tendency in order to try and identify the SE source.

As with all budget studies the interpretation of the individual components is difficult. In many cases no one particular parametrization stands out as providing the signature seen in the total tendency or SE. This is graphically illustrated for the zonally averaged budget in the extratropical boundary layer where the total tendency is a constant cooling in the vertical of -1.0 K/day, but the individual parametrized contributions show considerable vertical variation (e.g Boundary layer and convection schemes). One exception to this is the systematic cooling at tropopause level which is clearly dominated by the radiative terms. Possible ways forward with interpreting the individual contributions to the total budget may be

(i) To use independent information. For example the radiative budget can be contrasted with ERBE data.
(ii) To compare with heating rates from other model centres (ECMWF, NMC) over the same periods.
(iii) To contrast the budgets obtained under a variety of synoptic situations, such as when diabatic

heating is known to be particularly large. This may give clearer signals to deficiencies in particular parametrizations.

Despite the drawbacks of the technique a number of conclusions have been drawn regarding the UM thermal budget and the growth of SE in temperature. The main SE in temperature are given below with their possible causes listed in order of importance

1. The systematic cooling maxima in the extratropics:

- Insufficient parametrized diabatic heating in the Pacific and Atlantic stormtacks.
  - -Too little condensational heating due to large-scale cloud scheme ?
  - -Too little convective heating above the boundary layer ?
  - -Too much evaporative cooling due to dynamical precipitation in the stormtracks ?
  - - Missing parametrization - Slantwise convection?

2. The cooling in the subtropical regions:

- Imbalance between the large cooling due to the parametrizations and a smaller adiabatic warming in the descending branch of the Hadley cell - Too strong radiative cooling ?

3. The cooling maxima at the tropical tropopause:

- Too strong radiative cooling - high cloud distribution?.

4. Warming in the tropics over Indonesia, Sahel and Amazon regions - largest in July.

- Convective heating too intense?

5. Warming off the western continents at 850mb.

- Problems maintaining sufficient stratocumulus and stratus cloud near the coast.

6. Cooling of the surface in NH winter.

- Surface energy budget over land ?

Studying the time evolution of the thermal budget between T+00 and T+72 suggests that the cooling in the stormtracks is linked to the spin-up in the hydrological cycle. As forecasts progress there is an increase in cloud amount, relative humidity, and dynamic and convective rainfall in the extratropics. This is accompanied by an increase in latent heating due to the formation of large scale

cloud and an increase in convective heating. By T+72 this increased parametrized heating leads to a better balance between the diabatic and adiabatic components, although the model is still cooling at this forecast range. However the presence of a thermal imbalance at T+00 leads to the observed cooling which the model appears unable to recover from. At equilibrium we end up with a model which is both cooler and moister than analyses. Klinker (1992) shows that the ECMWF model has similar problems and suggests that the humidity in the analysis is underestimated, resulting in insufficient latent heating in extratropical cyclones. Clearly more diagnostic work is required to determine if the cooling in the UM is a model or analysis problem. Future work is planned with the single column version of the UM in order to test the sensitivity of the spin-up in the hydrological cycle and cooling of the model to variations both in initial moisture profiles and in alternative model formulations.

Finally, the two timestep integrations have proved very useful in identifying the physical processes responsible for the reduction in the cold bias in the extratropics upon the operational change to moisture diffusion. Given the inexpensive nature of the integrations it is suggested that similar diagnostics be calculated for all future parallel trials of proposed operational model changes. Future studies will apply similar diagnostic techniques to the momentum and moisture budget in the global UM.

Acknowledgements

Thanks to Frank Saunders in CF Division for providing figure 1 and Paul Berrisford at Reading University for providing the ECMWF diabatic heating estimates (Fig. 5(a) and (b)).

References

Boer, G.J. et. al 1991: An intercomparison of the climates simulated by 14 atmospheric general circulation models. *CAS/JSC WGNE report No. 15, WMO/TD - No. 425*

Bourke, W. et al. 1991: Systematic errors in extended range predictions. *CAS/JSC WGNE report No. 16, WMO/TD - No. 444*

Boville, B.A. 1985: The thermal balance of the NCAR Community Climate Model. *J.Atmos. Sci, 42, pp695-709*

Holopainen, E. 1987: Recent estimates of diabatic forcing on the planetary scale: a review. *ECMWF*

workshop proceedings on "Diabatic forcing", 30 Nov. - 2 Dec., pp29-58

Fortelius, C., and Holopainen, E.O. 1990: Comparison of energy source estimates derived from atmospheric circulation data with satellite measurements of net radiation. *J.Clim., 3, pp646-660*

Hoskins, B.J, Hsu,H.H., James,I.N., Masutani, M., Sardesmukh, P.D. and White, G.H. 1989: Diagnostics of the global atmospheric circulation : based on ECMWF analyses 1979-89. *WRCP-27,WMO/TD - No. 326*

Kanamitsu, M. and Saha, S. 1992: Budget analysis of the systematic error of the National Meteorological Center Medium Range Forecast model. *Research highlights of the NMC Development Division: 1989-1991, pp196-205*

Klinker, E. 1990: Investigation of systematic errors by relaxation experiments. *Q.J.R. Meteorol., 116, pp*573-594.

Klinker, E., and Sardesmukh, P.D. 1987: The diagnosis of systematic errors in numerical weather prediction models. *ECMWF workshop proceedings on "Diabatic forcing", 30 Nov. - 2 Dec., pp209-244.*

Klinker, E., and Sardesmukh, P.D. 1992: The diagnosis of mechanical dissipation in the atmosphere from large-scale balance requirements. *J.Atmos. Sci., 49, pp608-627.*

Klinker, E. 1992: Validation of the forcing in the ECMWF model. *In ECMWF Seminar proceedings on "Validation of models over Europe. Volume II".*

Milton, S.F. 1993: Surface energy balance in the Unified Model - comparison with NMC and ECMWF. *(Available from the author)*

Rawlins, F. 1992: Preliminary results of tests using pre-'climate frozen' physics at operational resolution. *FR Division working paper. No 138. (Available from FR division)*

Smith, R.N.B 1993: Experience and developments with the layer cloud and boundary layer mixing schemes in the U.K. Meteorological Office Unified Model. *In proceedings of an ECMWF workshop*

on "The parametrization of cloud topped boundary layers".

Appendix A - Determination of heating increments in the Unified Model.

The schematic diagram below shows the order in which routines are called in the Unified Model and the thermodynamic quantities (T= temperature, q_C= cloud water content) which are diagnosed in order to calculate the thermal budget.

	Large scale precipitation (LPPN)	$\Rightarrow q_{C1}$ (LPPN)
Timestep 1	⇓	
	Convection (CONV)	$\Rightarrow T_1$ (CONV)
	Dynamics (DYN)	
	⇓	
	Large scale cloud (CLOUD)	$\Rightarrow T_2$ (DYN + CLOUD)
	⇓	q_{C2} (DYN + CLOUD)
	Radiation (SW + LW)	$\Rightarrow T_2$ (SW)
	⇓	T_2 (LW)
	Boundary Layer (BL)	$\Rightarrow T_2$ (BL)
Timestep 2	⇓	
	Large scale precipitation	$\Rightarrow T_2$ (LPPN)
	⇓	
	Convection	$\Rightarrow T_2$ (CONV)
	⇓	
	Vertical diffusion	
	⇓	
	Gravity wave drag	

The heating increments are calculated by differencing the temperatures after each routine , for example;

$$\Delta T \text{ (ALL ROUTINES)} = T_2 \text{ (CONV)} - T_1 \text{ (CONV)}$$

$$\Delta T \text{ (DYN + CLOUD)} = T_2 \text{ (DYN + CLOUD)} - T_1 \text{ (CONV)}$$

These are then multiplied by the number of timesteps in a day to give heating increments in K/day.

Owing to the fact that the dynamics scheme uses the cloud conserved variable T_L (Liquid water temperature), the increment to temperature from the dynamics scheme cannot be directly calculated. It is determined by calculating the heating increment due to L.S. cloud from the change in q_C and then taking this away from the dynamics+cloud heating increment, as shown below;

$$\Delta T \text{ (CLOUD)} = L/C_P \{q_{C2} \text{ (DYN + CLOUD)} - q_{C1} \text{ (LPPN)}\}$$

$$\Delta T \text{ (DYN)} = \Delta T \text{ (DYN + CLOUD)} - \Delta T \text{ (CLOUD)}$$

Appendix B - Differences in Parametrizations in Operational and Climate Configurations.

Boundary Layer

Operational - local mixing criterion for temperature and moisture

Climate - local and non-local mixing for temperature and moisture

Convection

Operational - Updraught only

Climate - Updraughts and Downdraughts included.

Radiation

Operational- ECMWF LW transmissivities, 16 cloud levels in SW and LW, random overlap.

Climate - 3 cloud layers (random overlap) in SW, maximum/random overlap in LW.

Cloud

Operational - Liquid water temperature is dependent variable.

Triangular distribution function to derive statistical distribution of total water.

Climate - Temperature is dependent variable.

Alternative method of solution for cloud and humidity.

Top hat distribution function to derive statistical distribution of total water.

Large-Scale Precipitation

Operational - Standard scheme.

Climate - Threshold in cloud water reduced over the ocean from 8×10^{-4} to 2×10^{-4} kg/kg

Critical RH thresholds altered in lowest 3 model levels.

Increased evaporation of snow. (also for convective precipitation).

Flux divergence form for ice precipitation (independent of vertical resolution).

Vertical diffusion

Operational - Applied between 30°N - 30°S and levels 8-14.

Climate - Not applied.

Horizontal Diffusion

Operational - ∇^4 - momentum , ∇^4 - moisture (since March 1993)

Climate - ∇^6 - momentum, ∇^4 - moisture (coefficient half the value of the Operational)

Figure captions

Figure 1 Zonally averaged cross sections of systematic error (SE) in temperature for December 1992 from operational global UM forecasts at T+72. The SE is the mean difference between operational forecasts and analyses. Contour interval is 0.5 K and negative values are shaded.

Figure 2 (a) Systematic error in temperature at 850mb for December 1992 from operational global UM forecasts at T+72. (b) as (a) but at 250mb. (c) Monthly averaged MSLP for December 1992 from T+00 unified model operational analyses. Contour intervals are 1 K in (a) and (b) and 4mb in (c). Negative values are shaded.

Figure 3 Zonally averaged cross sections of the Unified Model mean thermal budget for December 1992. (a) Total tendency in temperature due to all model routines. (b) contribution to total tendency from the model dynamics (adiabatic component) shown with the sign reversed. (c) as (b) but for the model parametrizations (diabatic component). Contour interval is 0.4 K/day in (a) and 0.5 K/day in (b) and (c). Negative contours are dashed.

Figure 4 Zonally avergaed cross section of the trend in temperature for December 1992 calculated from Unified Model operational analyses. Contour interval is 0.1 K/day and negative values are shaded.

Figure 5 Zonally averaged cross sections of estimates of diabatic heating from (a) ECMWF analyses for 1-15 December 1992, (b) as (a) but for 16-31 December 1992, and (c) from "final" initialised FGGE level IIIb ECMWF analyses for February 1979 (Taken from Fortelius and Holopainen, 1990). Contour interval for (a) and (b) is 0.4 K/day and positive values are shaded. Contour interval for (c) is 0.5 K/day and heavy shading denotes positive values.

Figure 6 Zonally averaged cross sections of the mean heating rate for December 1992 due to parametrizations of (a) SW radiation, (b) LW radiation, and (c) Total radiation, SW+LW. Contour interval is 0.2 K/day and negative contours are dashed.

Figure 7 As figure 6 but for (a) Boundary layer scheme, (b) Convection, and (c) Large-scale precipitation. Contour intervals are 2.0, 0.5, and 0.2 K/day respectively.

Figure 8 Zonally averaged cross sections of (a) the mean heating rate for December 1992 due to the parametrization of large-scale cloud, (b) Model layer cloud fraction, and (c) Model convective cloud fraction. Contour intervals are 0.2 K/day, 4%, and 2% respectively. Negative contours are dashed.

Figure 9 Zonally averaged vertical profiles (K/day) of for 40°N during December 1992 for (a) Total tendency in temperature, (b) Parametrized and (-)Dynamical tendencies, and (c) tendencies due to individual model parametrizations.

Figure 10 As figure 9 but for 5°S.

Figure 11 As figure 9 but for 42°S.

Figure 12 Mean temperature budget for December 1992 at model level 4 ($\eta = 0.867$, $\sim$ 850mb). (a) Total tendency in temperature due to all model routines. (b) contribution to total

tendency from the model dynamics (adiabatic component) shown with the sign reversed. (c) as (b) but for the model parametrizations (diabatic component). Contour interval is 1 K/day in (a) and 2 K/day in (b) and (c). Negative values are shaded.

Figure 13 Mean heating rate for December 1992 due to parametrizations of (a) SW radiation, (b) LW radiation, and (c) Total radiation, SW+LW. Contour interval is 1.0 K/day and negative values are shaded.

Figure 14 As figure 13 but for (a) Boundary layer, (b) Convection, (c) Large-scale precipitation, and (d) Large-scale cloud. Contour intervals are 1, 2, 1, and 2 K/day respectively. Negative values are shaded.

Figure 15 Zonally averaged cross sections of total tendency in temperature for February 1993 using (a) ∇^2 moisture diffusion, (b) ∇^4 moisture diffusion, and for (c) ∇^4 minus ∇^2. Contour interval is 0.4 K/day for (a) and (b) and 0.1 K/day for (c). Negative contours are dashed.

Figure 16 As figure 15 but for model parametrized heating rates. Contour interval is 0.5 K/day for (a) and (b) and 0.1 K/day for (c). Negative contours are dashed.

Figure 17 As figure 15 but for model (-)dynamical heating rates. Contour interval is 0.5 K/day for (a) and (b) and 0.1 K/day for (c). Negative contours are dashed.

Figure 18 As figure 15 but for model heating rates from the convection scheme. Contour interval is 0.5 K/day for (a) and (b) and 0.1 K/day for (c). Negative contours are dashed.

Figure 19 As figure 15 but for model heating rates from the convection scheme. Contour interval is 0.5 K/day for (a) and (b) and 0.1 K/day for (c). Negative contours are dashed.

Figure 20 Zonally averaged cross sections of the Unified Model mean thermal budget for 1-11 July 1992 from T+00. (a) Total tendency in temperature due to all model routines. (b) contribution to total tendency from the model dynamics (adiabatic component) shown with the sign reversed. (c) as (b) but for the model parametrizations (diabatic component). Contour interval is 0.4 K/day in (a) and 0.5 K/day in (b) and (c). Negative contours are dashed.

Figure 21 As figure 20 but for integrations from T+72 model dumps.

Figure 22 Zonally averaged cross sections of mean heating rate for 1-11 July 1992 from parametrization of large-scale cloud for (a) integrations run from T+00 (b) intergations run from T+72 (c) difference T+72 minus T+00. Contour interval is 0.2 K/day. Negative contours are dashed.

Figure 23 As figure 22 but for parametrization of convection. Contour interval is 0.5 K/day in (a) and (b) and 0.2 K/day in (c). Negative contours are dashed.

Figure 24 As figure 22 but for parametrization of radiation (SW+LW). Contour interval is 0.2 K/day in (a) and (b) and 0.1 K/day in (c). Negative contours are dashed.

Figure 25 Large scale cloud fraction from July integrations. (a) T+00 (b) T+72 (c) difference, T+72 minus T+00. Contour interval is 4% for (a) and (b) and 2% for (c). Negative contours are dashed.

Figure 26 Hydrological budget at T+00 and T+72 for July 93 two timestep integrations. (a) Total precipitation (b) Evaporation (c)Dynamic rainfall (d) Convective rainfall. Units are kg/kg/day.

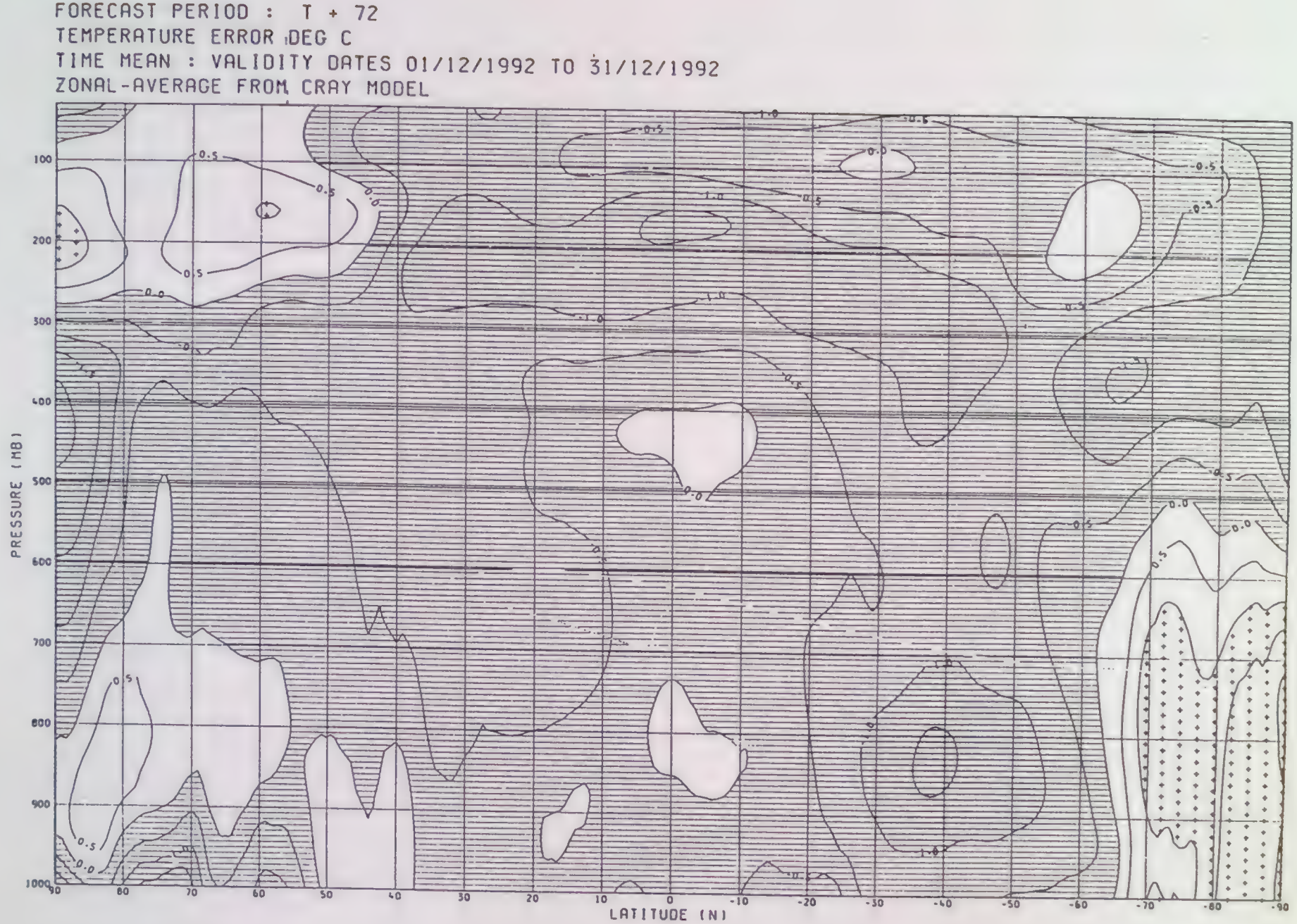
FORECAST PERIOD : T + 72
TEMPERATURE ERROR DEG C
TIME MEAN : VALIDITY DATES 01/12/1992 TO 31/12/1992
ZONAL-AVERAGE FROM CRAY MODEL
PRESSURE (MB)
100
200
300
400
500
600
700
800
900
1000
90 80 70 60 50 40 30 20 10 0 -10 -20 -30 -40 -50 -60 -70 -80 -90
LATITUDE (N)

Figure 1

(a)

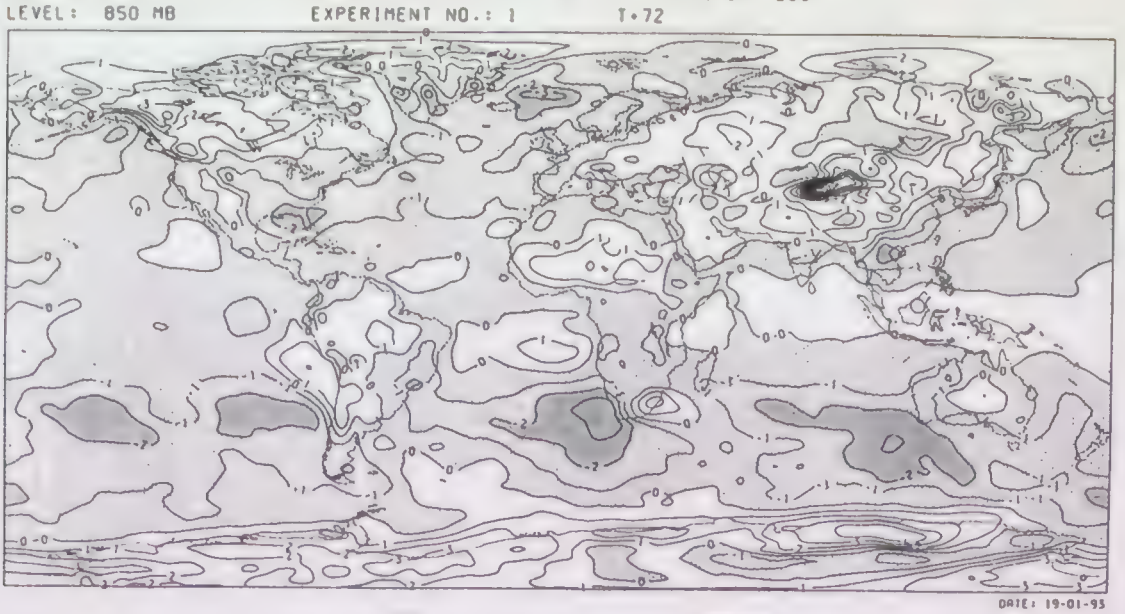
UM MAIN T+72 - T+00 SYSTEMATIC ERRORS - DECEMBER 92
TEMPERATURE DIFFERENCE (DEGREES K)
AVERAGE FROM 0Z ON 1/12/1992 DAY 336 TO 0Z ON 31/12/1992 DAY 366
LEVEL: 850 MB EXPERIMENT NO.: 1 T+72
DATE: 19-01-93

(b)

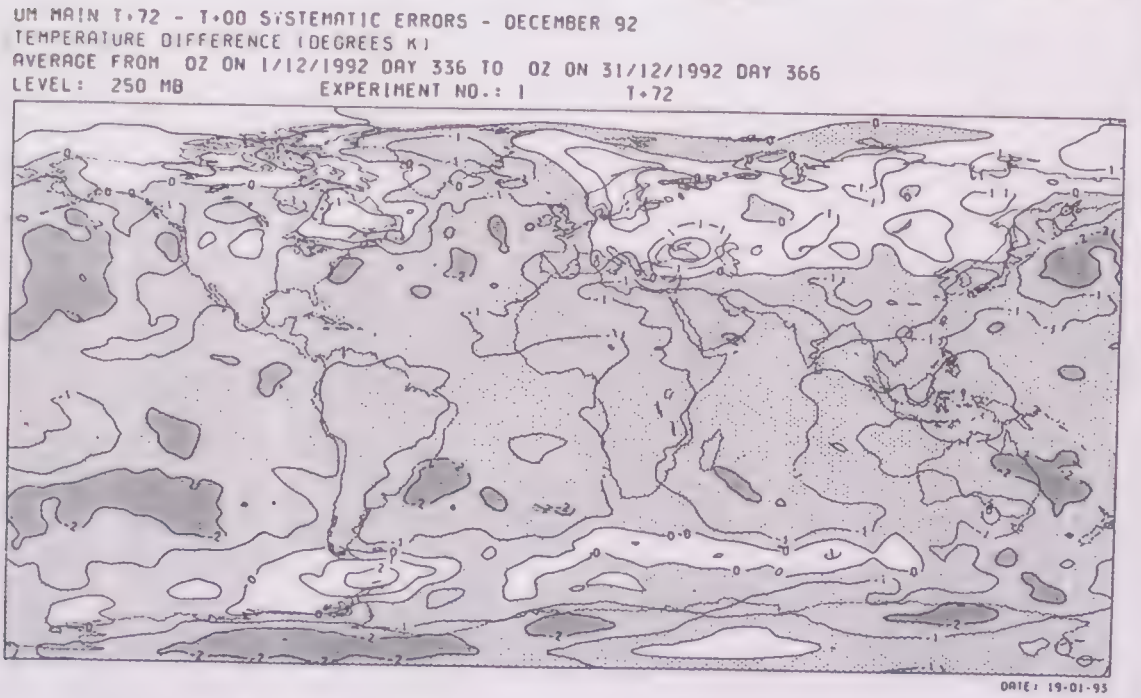
UM MAIN T+72 - T+00 SYSTEMATIC ERRORS - DECEMBER 92
TEMPERATURE DIFFERENCE (DEGREES K)
AVERAGE FROM 0Z ON 1/12/1992 DAY 336 TO 0Z ON 31/12/1992 DAY 366
LEVEL: 250 MB EXPERIMENT NO.: 1 T+72
DATE: 19-01-93

(c)

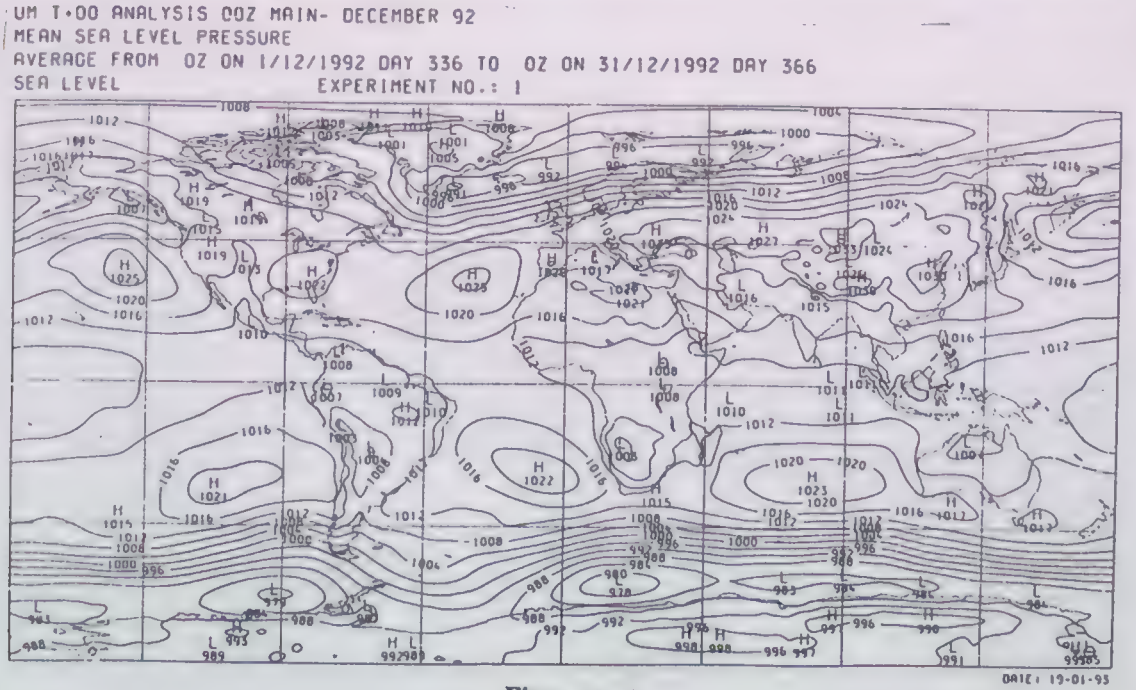
UM T+00 ANALYSIS 00Z MAIN- DECEMBER 92
MEAN SEA LEVEL PRESSURE
AVERAGE FROM 0Z ON 1/12/1992 DAY 336 TO 0Z ON 31/12/1992 DAY 366
SEA LEVEL EXPERIMENT NO.: 1
DATE: 19-01-93

Figure 2

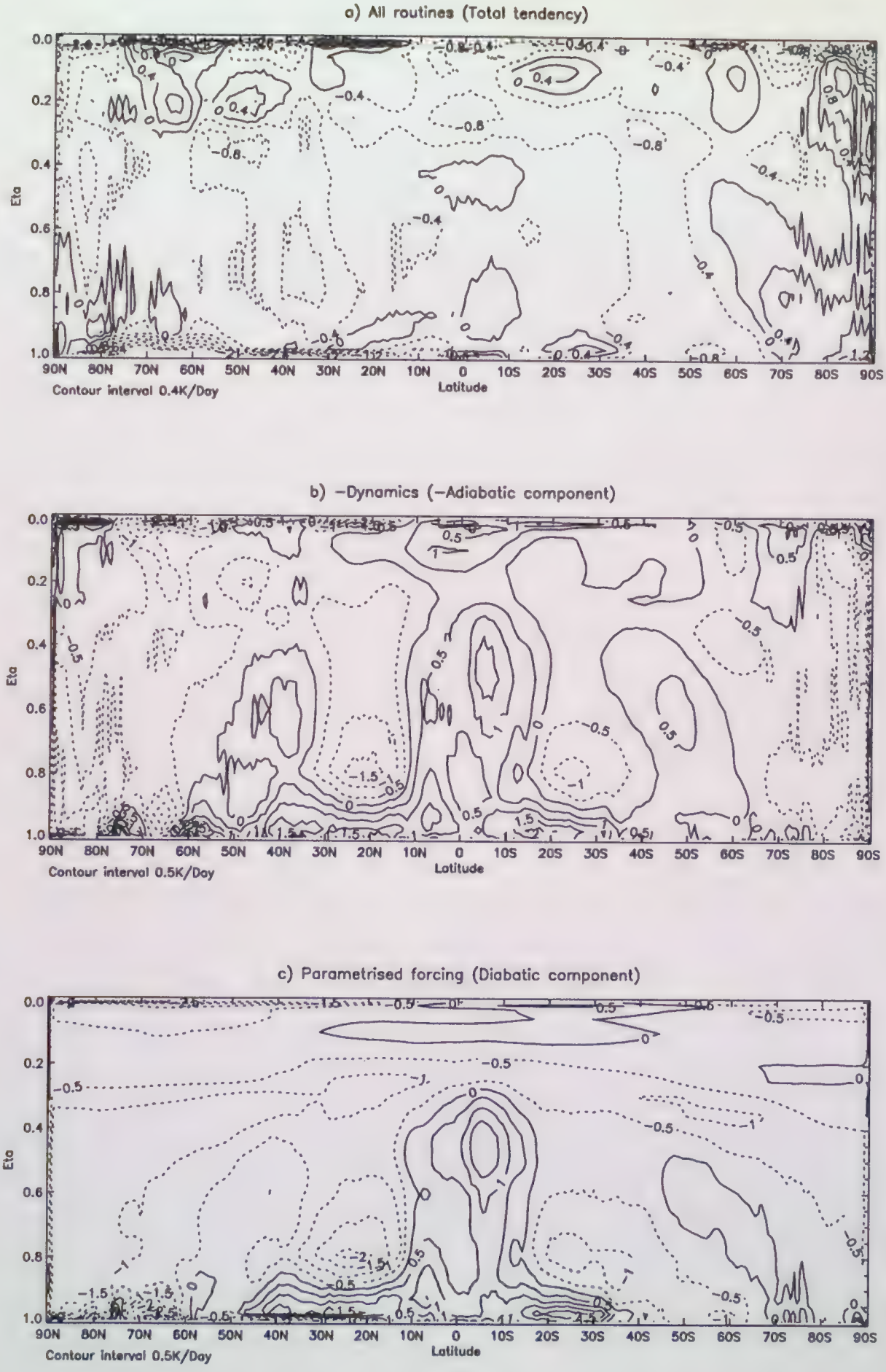
a) All routines (Total tendency)
Eta
Latitude
Contour interval 0.4K/Day
b) −Dynamics (−Adiabatic component)
Eta
Latitude
Contour interval 0.5K/Day
c) Parametrised forcing (Diabatic component)
Eta
Latitude
Contour interval 0.5K/Day

Figure 3

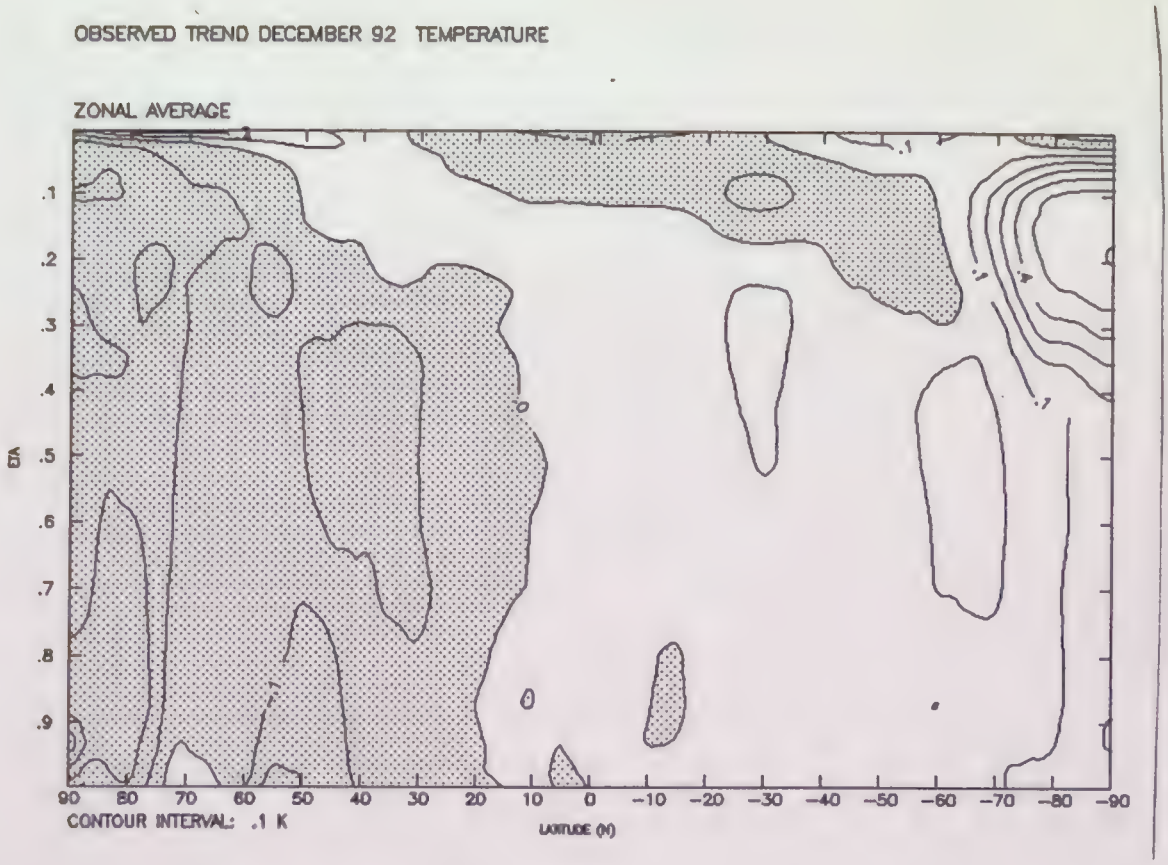
OBSERVED TREND DECEMBER 92 TEMPERATURE
ZONAL AVERAGE
.1
.2
.3
.4
.5
.6
.7
.8
.9
90 80 70 60 50 40 30 20 10 0 -10 -20 -30 -40 -50 -60 -70 -80 -90
CONTOUR INTERVAL: .1 K
LATITUDE (N)

Figure 4

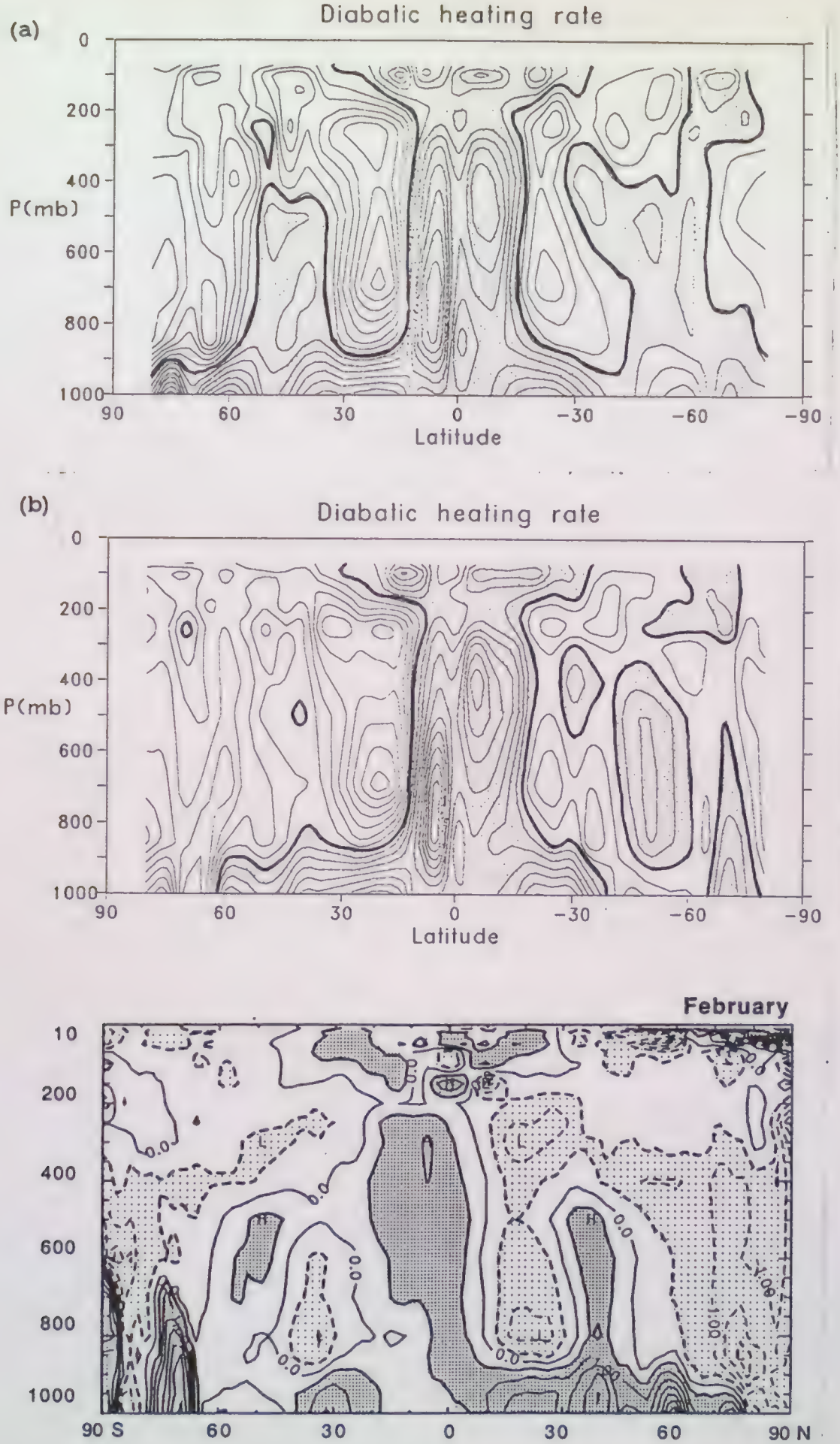
(a)
Diabatic heating rate
P(mb)
0
200
400
600
800
1000
90
60
30
0
-30
-60
-90
Latitude
(b)
Diabatic heating rate
P(mb)
0
200
400
600
800
1000
90
60
30
0
-30
-60
-90
Latitude
February
10
200
400
600
800
1000
90 S
60
30
0
30
60
90 N

Figure 5

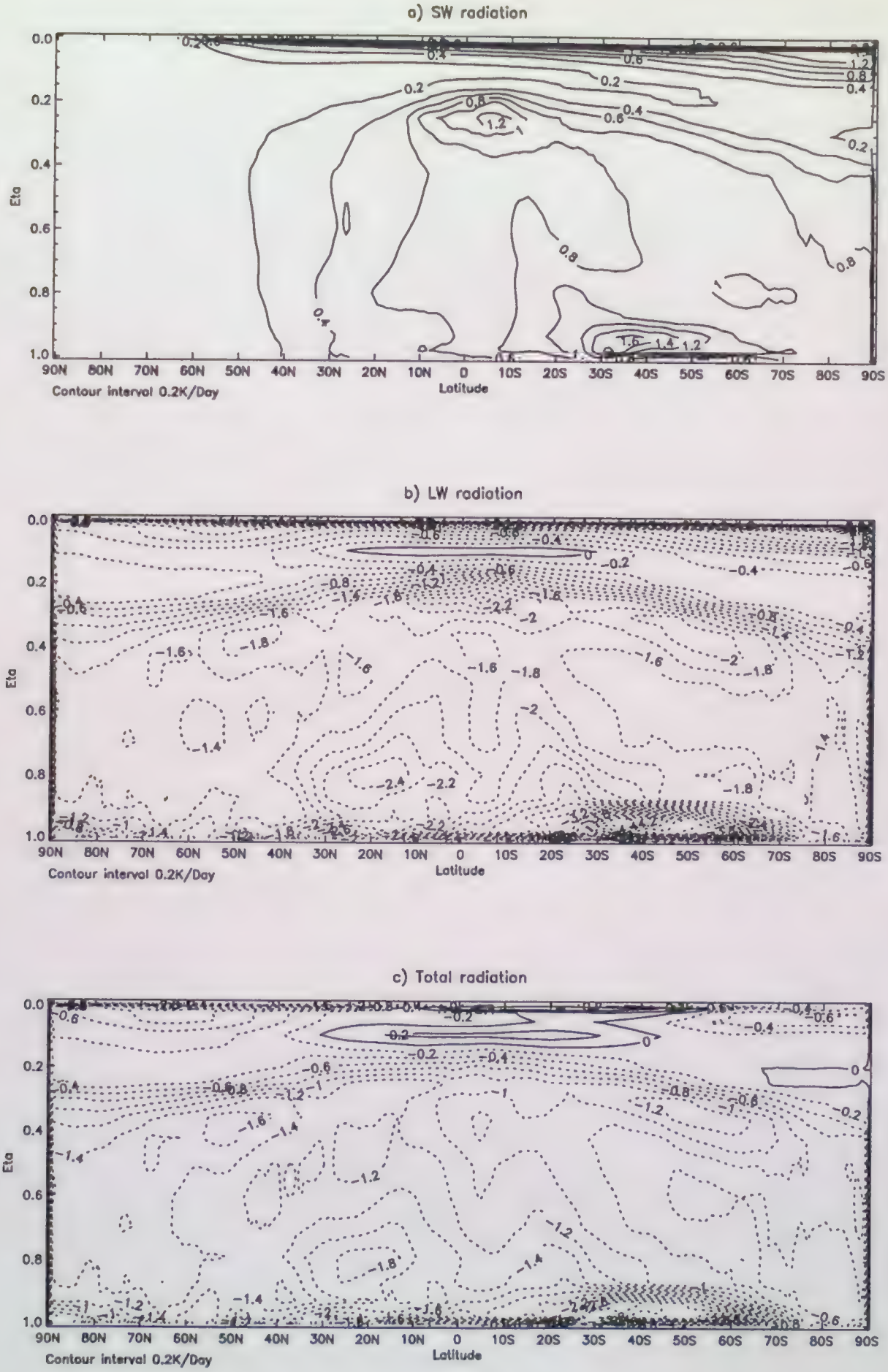
a) SW radiation
b) LW radiation
c) Total radiation
Eta
0.0
0.2
0.4
0.6
0.8
1.0
90N 80N 70N 60N 50N 40N 30N 20N 10N 0 10S 20S 30S 40S 50S 60S 70S 80S 90S
Latitude
Contour interval 0.2K/Day

Figure 6

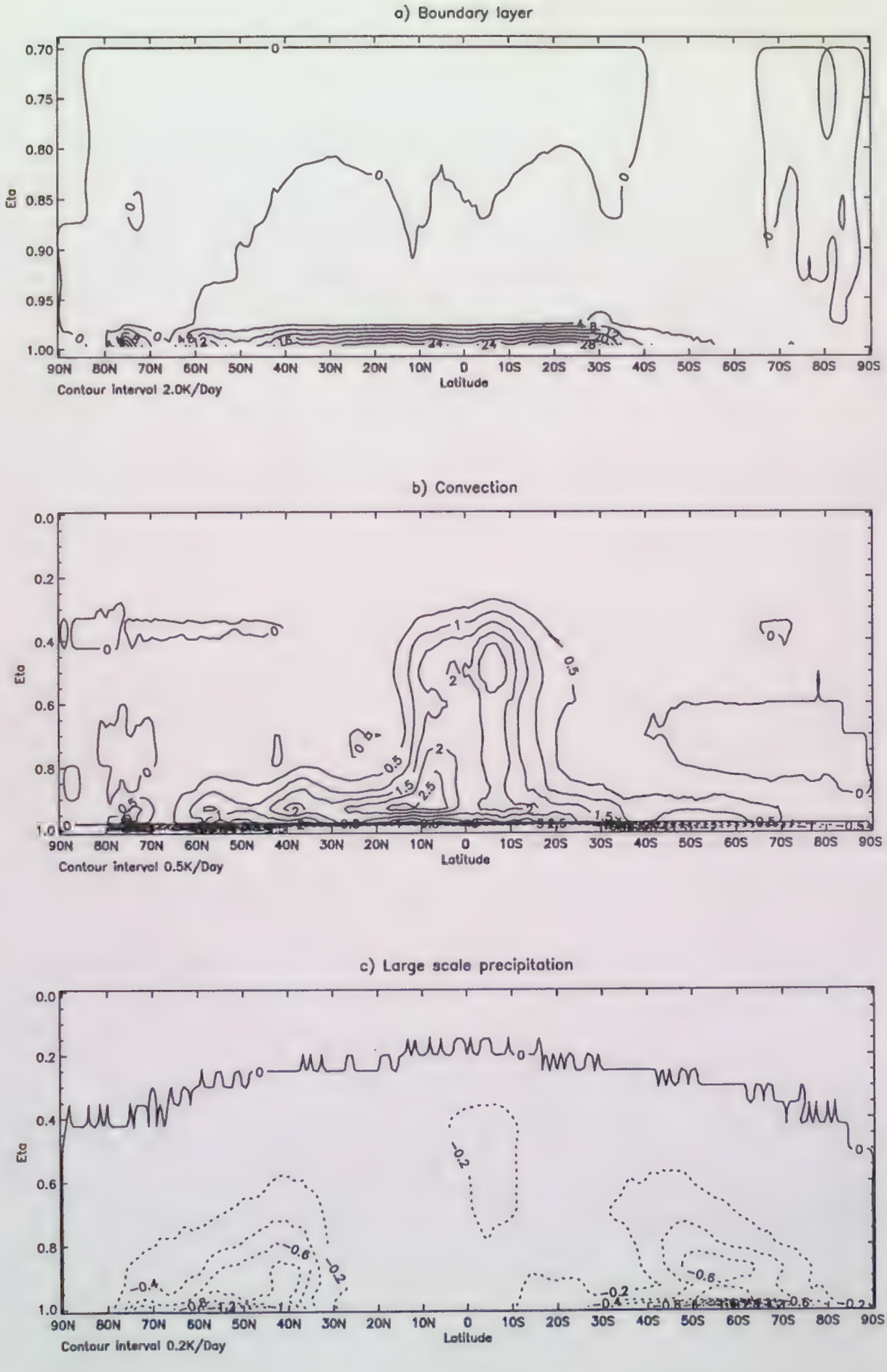
a) Boundary layer
Eta
0.70
0.75
0.80
0.85
0.90
0.95
1.00
90N 80N 70N 60N 50N 40N 30N 20N 10N 0 10S 20S 30S 40S 50S 60S 70S 80S 90S
Latitude
Contour interval 2.0K/Day
b) Convection
Eta
0.0
0.2
0.4
0.6
0.8
1.0
90N 80N 70N 60N 50N 40N 30N 20N 10N 0 10S 20S 30S 40S 50S 60S 70S 80S 90S
Latitude
Contour interval 0.5K/Day
c) Large scale precipitation
Eta
0.0
0.2
0.4
0.6
0.8
1.0
90N 80N 70N 60N 50N 40N 30N 20N 10N 0 10S 20S 30S 40S 50S 60S 70S 80S 90S
Latitude
Contour interval 0.2K/Day

Figure 7

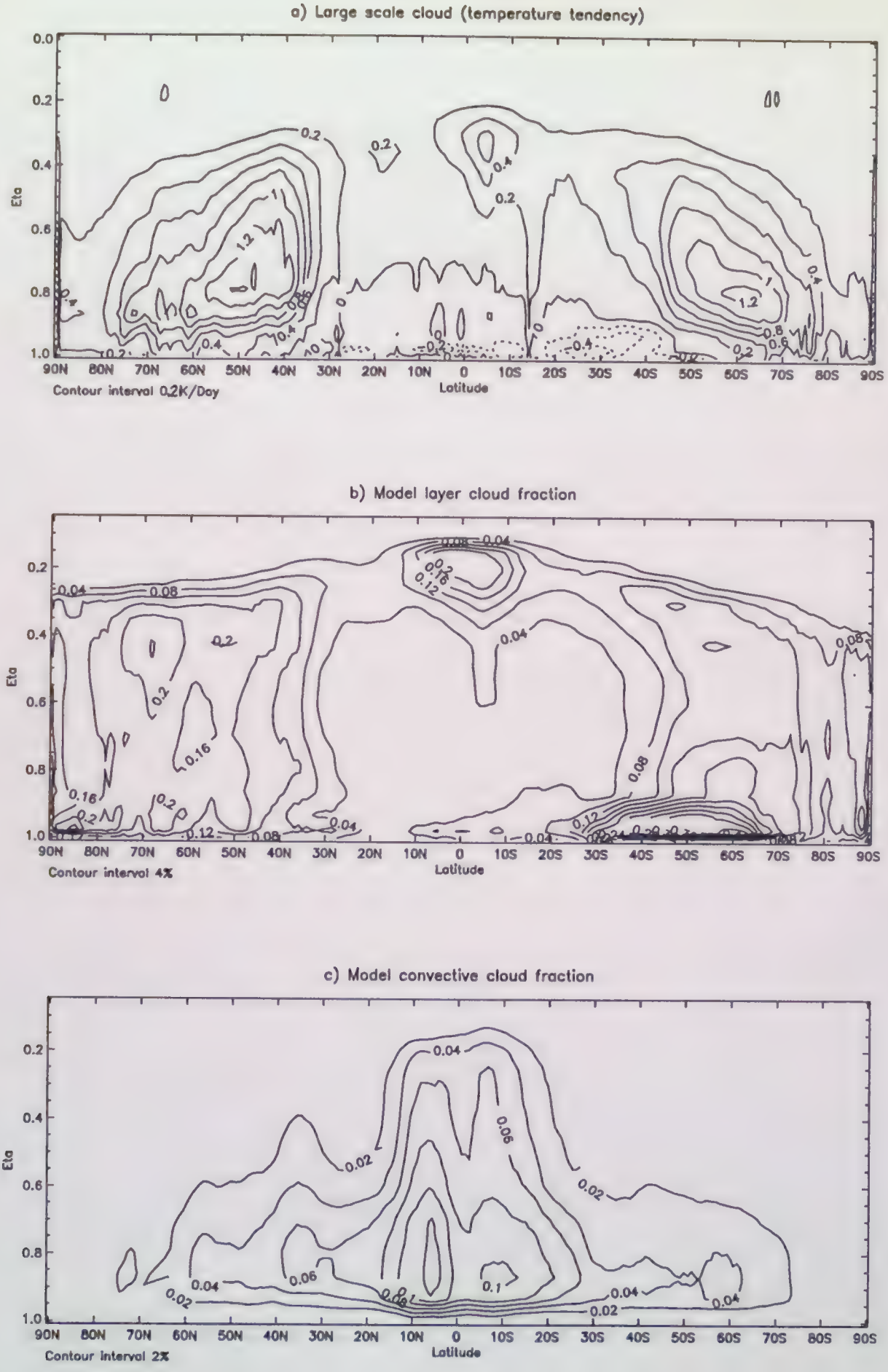
a) Large scale cloud (temperature tendency)
Eta
Latitude
90N 80N 70N 60N 50N 40N 30N 20N 10N 0 10S 20S 30S 40S 50S 60S 70S 80S 90S
Contour interval 0.2K/Day
b) Model layer cloud fraction
Eta
Latitude
Contour interval 4%
c) Model convective cloud fraction
Eta
Latitude
Contour interval 2%

Figure 8

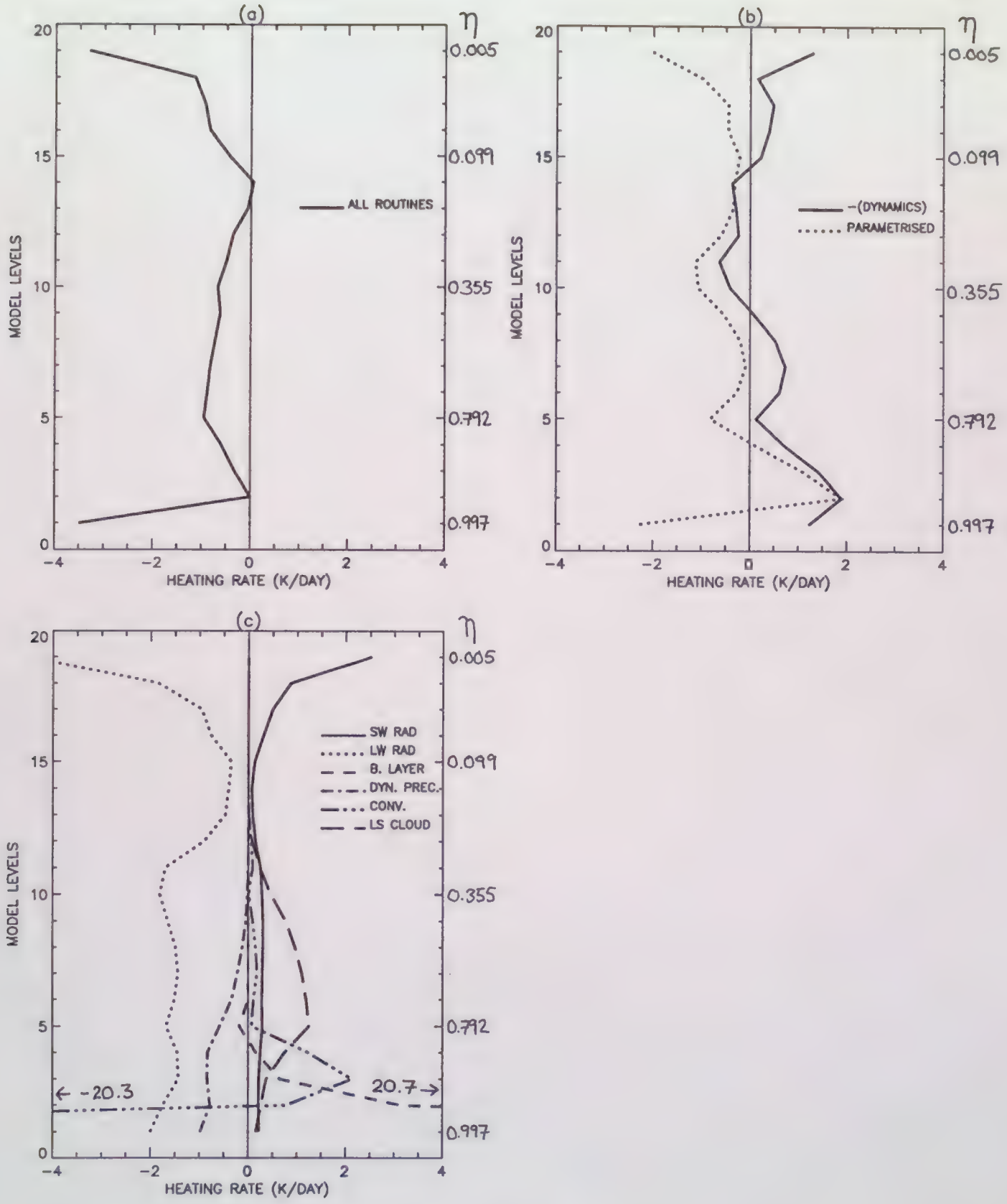
(a)
(b)
(c)
η
0.005
0.099
0.355
0.792
0.997
MODEL LEVELS
HEATING RATE (K/DAY)
ALL ROUTINES
-(DYNAMICS)
PARAMETRISED
SW RAD
LW RAD
B. LAYER
DYN. PREC.
CONV.
LS CLOUD
← -20.3
20.7→

Figure 9

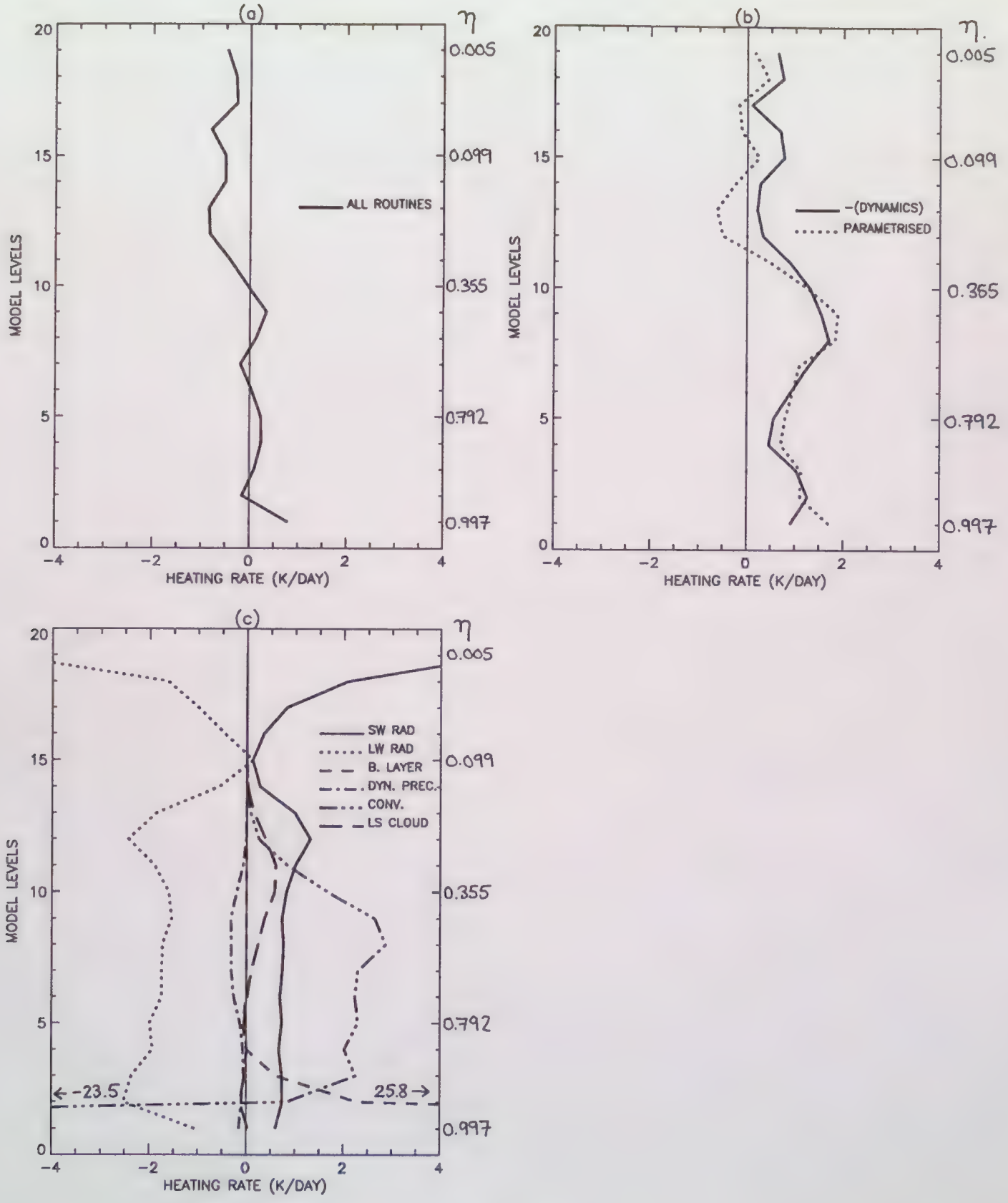
(a)
η
0.005
0.099
0.355
0.792
0.997
ALL ROUTINES
MODEL LEVELS
HEATING RATE (K/DAY)
(b)
η
0.005
0.099
0.365
0.792
0.997
-(DYNAMICS)
PARAMETRISED
MODEL LEVELS
HEATING RATE (K/DAY)
(c)
η
0.005
0.099
0.355
0.792
0.997
SW RAD
LW RAD
B. LAYER
DYN. PREC.
CONV.
LS CLOUD
← -23.5
25.8 →
MODEL LEVELS
HEATING RATE (K/DAY)

Figure 10

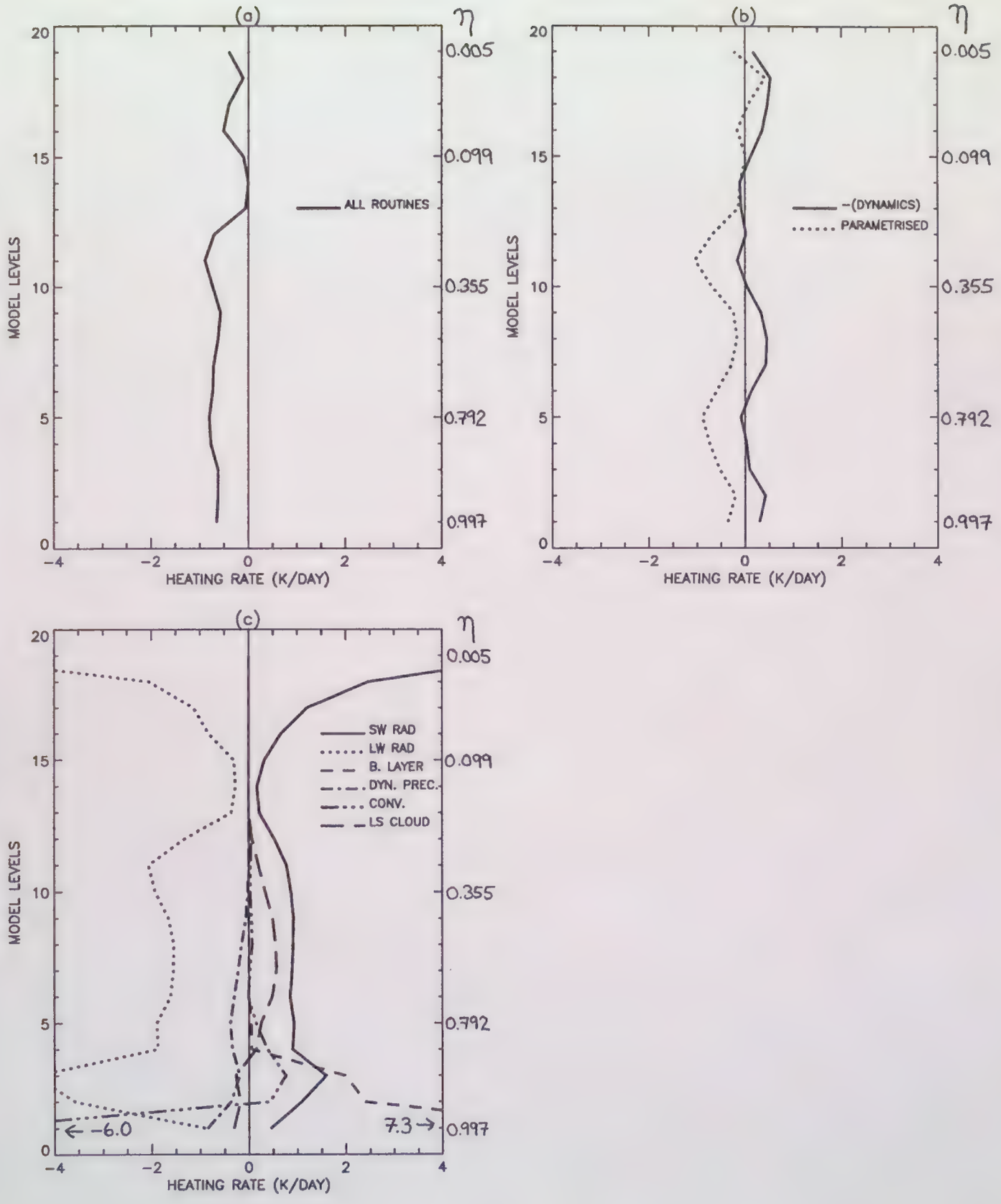
(a)
(b)
(c)
η
0.005
0.099
0.355
0.792
0.997
MODEL LEVELS
HEATING RATE (K/DAY)
ALL ROUTINES
-(DYNAMICS)
PARAMETRISED
SW RAD
LW RAD
B. LAYER
DYN. PREC.
CONV.
LS CLOUD
← -6.0
7.3 →

Figure 11

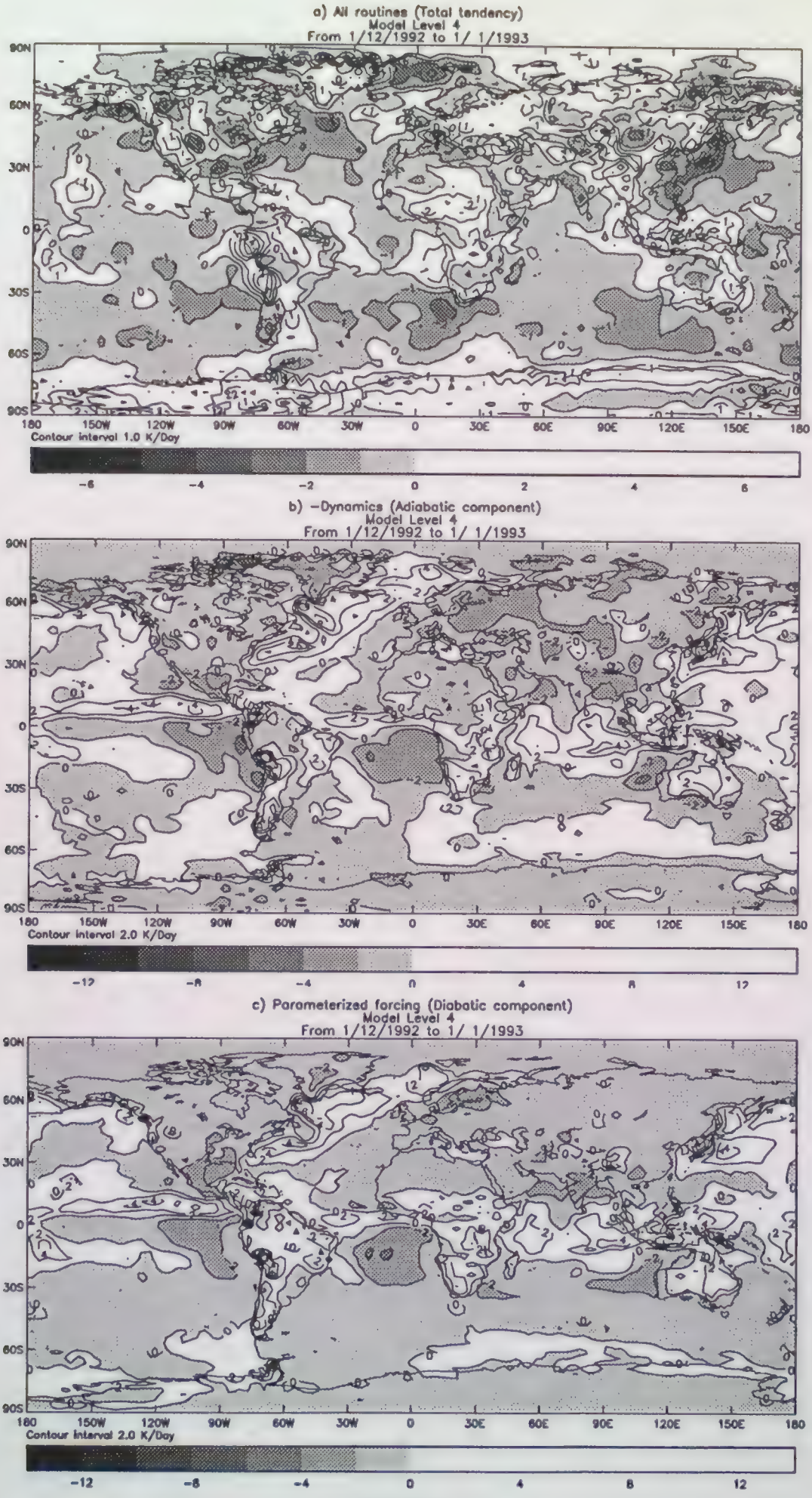
a) All routines (Total tendency)
Model Level 4
From 1/12/1992 to 1/ 1/1993
90N
60N
30N
0
30S
60S
90S
180 150W 120W 90W 60W 30W 0 30E 60E 90E 120E 150E 180
Contour interval 1.0 K/Day
-6 -4 -2 0 2 4 6
b) -Dynamics (Adiabatic component)
Model Level 4
From 1/12/1992 to 1/ 1/1993
90N
60N
30N
0
30S
60S
90S
180 150W 120W 90W 60W 30W 0 30E 60E 90E 120E 150E 180
Contour interval 2.0 K/Day
-12 -8 -4 0 4 8 12
c) Parameterized forcing (Diabatic component)
Model Level 4
From 1/12/1992 to 1/ 1/1993
90N
60N
30N
0
30S
60S
90S
180 150W 120W 90W 60W 30W 0 30E 60E 90E 120E 150E 180
Contour interval 2.0 K/Day
-12 -8 -4 0 4 8 12

Figure 12

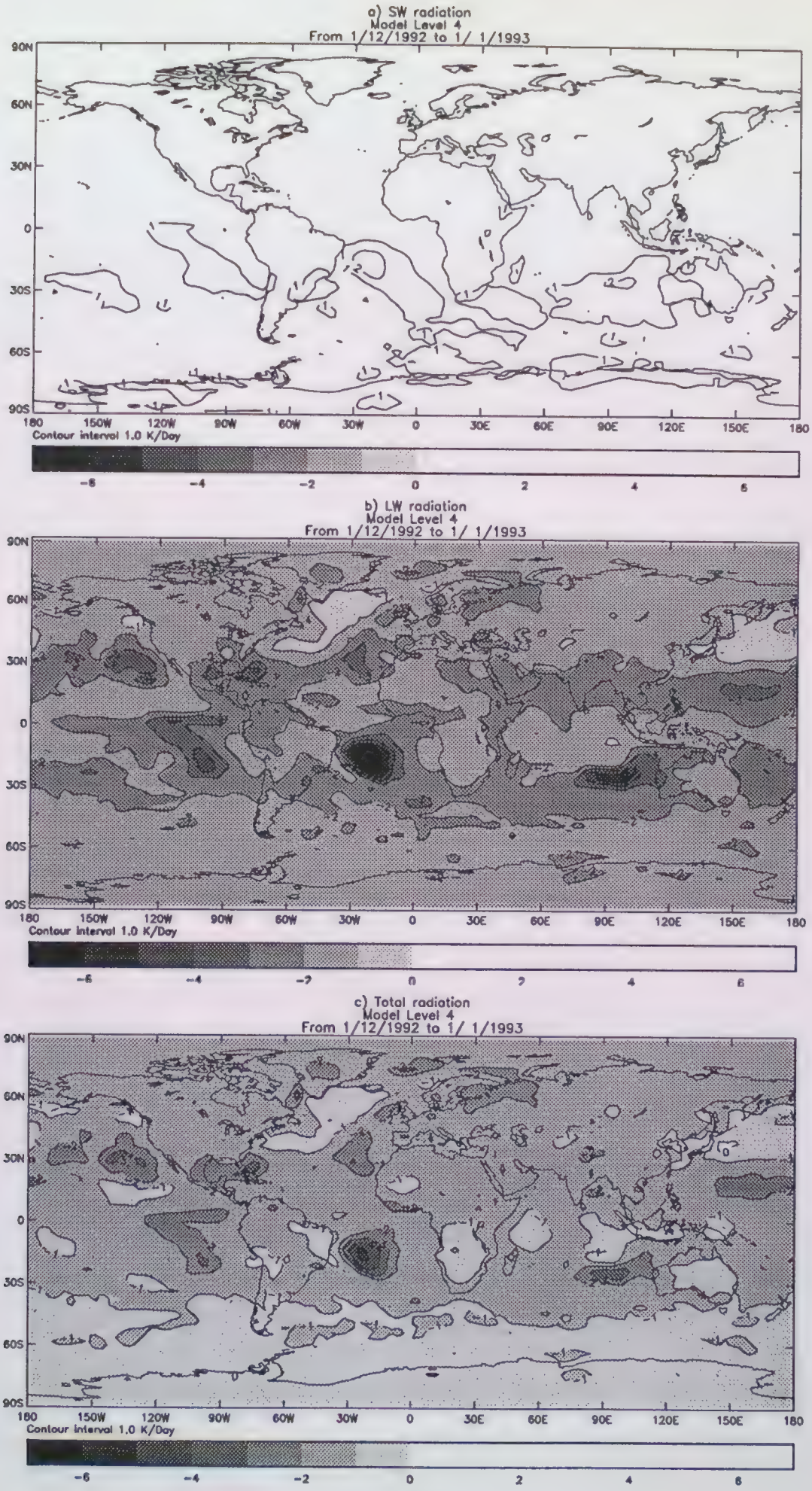
a) SW radiation
Model Level 4
From 1/12/1992 to 1/ 1/1993
90N
60N
30N
0
30S
60S
90S
180 150W 120W 90W 60W 30W 0 30E 60E 90E 120E 150E 180
Contour interval 1.0 K/Day
-6 -4 -2 0 2 4 6
b) LW radiation
Model Level 4
From 1/12/1992 to 1/ 1/1993
90N
60N
30N
0
30S
60S
90S
180 150W 120W 90W 60W 30W 0 30E 60E 90E 120E 150E 180
Contour interval 1.0 K/Day
-6 -4 -2 0 2 4 6
c) Total radiation
Model Level 4
From 1/12/1992 to 1/ 1/1993
90N
60N
30N
0
30S
60S
90S
180 150W 120W 90W 60W 30W 0 30E 60E 90E 120E 150E 180
Contour interval 1.0 K/Day
-6 -4 -2 0 2 4 6

Figure 13

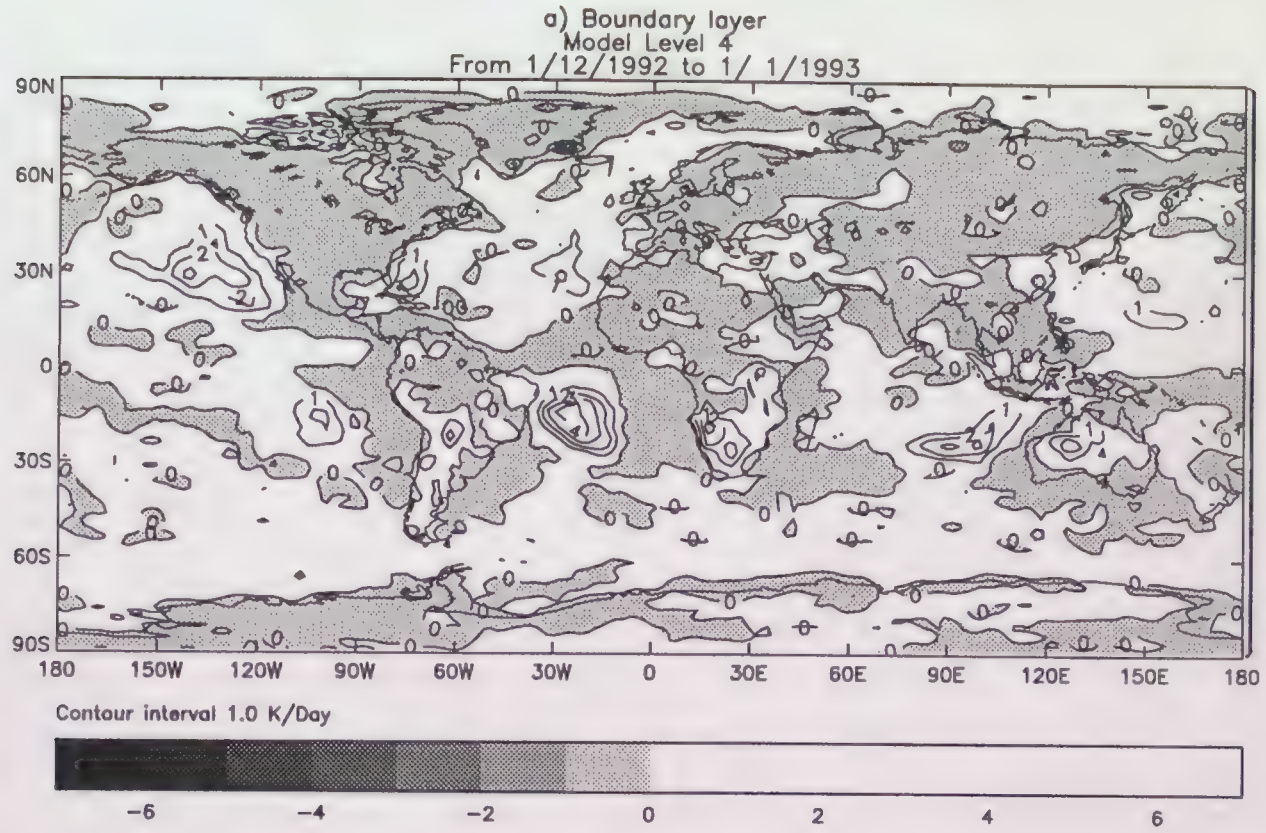
a) Boundary layer
Model Level 4
From 1/12/1992 to 1/ 1/1993
90N
60N
30N
0
30S
60S
90S
180
150W
120W
90W
60W
30W
0
30E
60E
90E
120E
150E
180
Contour interval 1.0 K/Day
-6
-4
-2
0
2
4
6

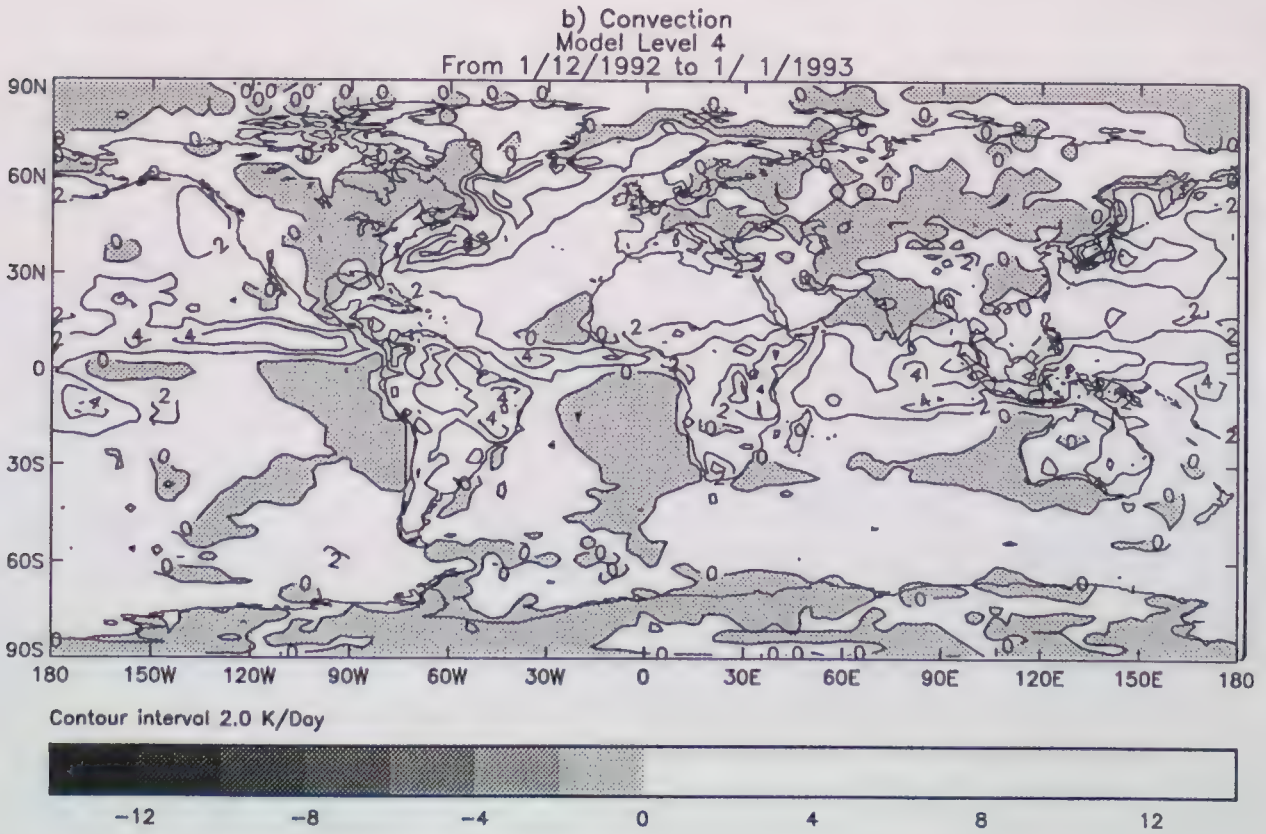
b) Convection
Model Level 4
From 1/12/1992 to 1/ 1/1993
90N
60N
30N
0
30S
60S
90S
180
150W
120W
90W
60W
30W
0
30E
60E
90E
120E
150E
180
Contour interval 2.0 K/Day
-12
-8
-4
0
4
8
12

Figure 14

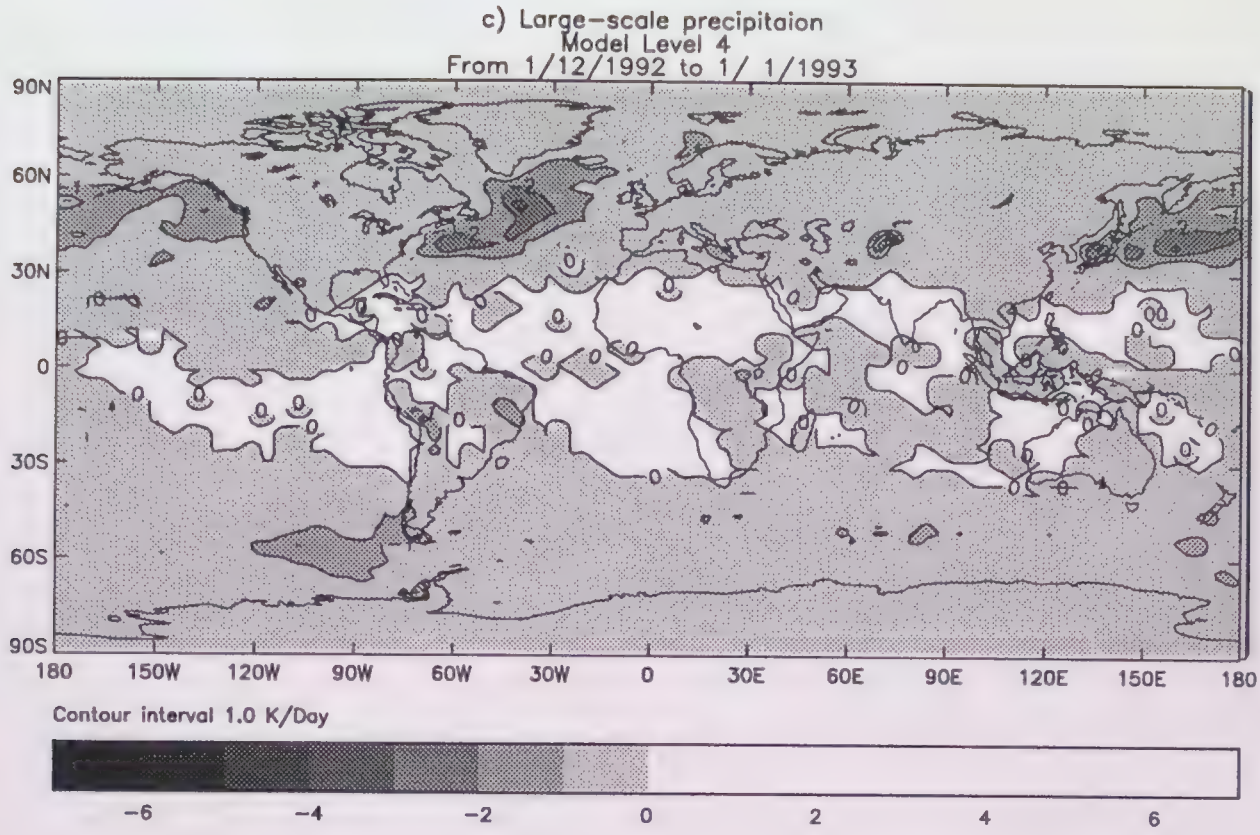

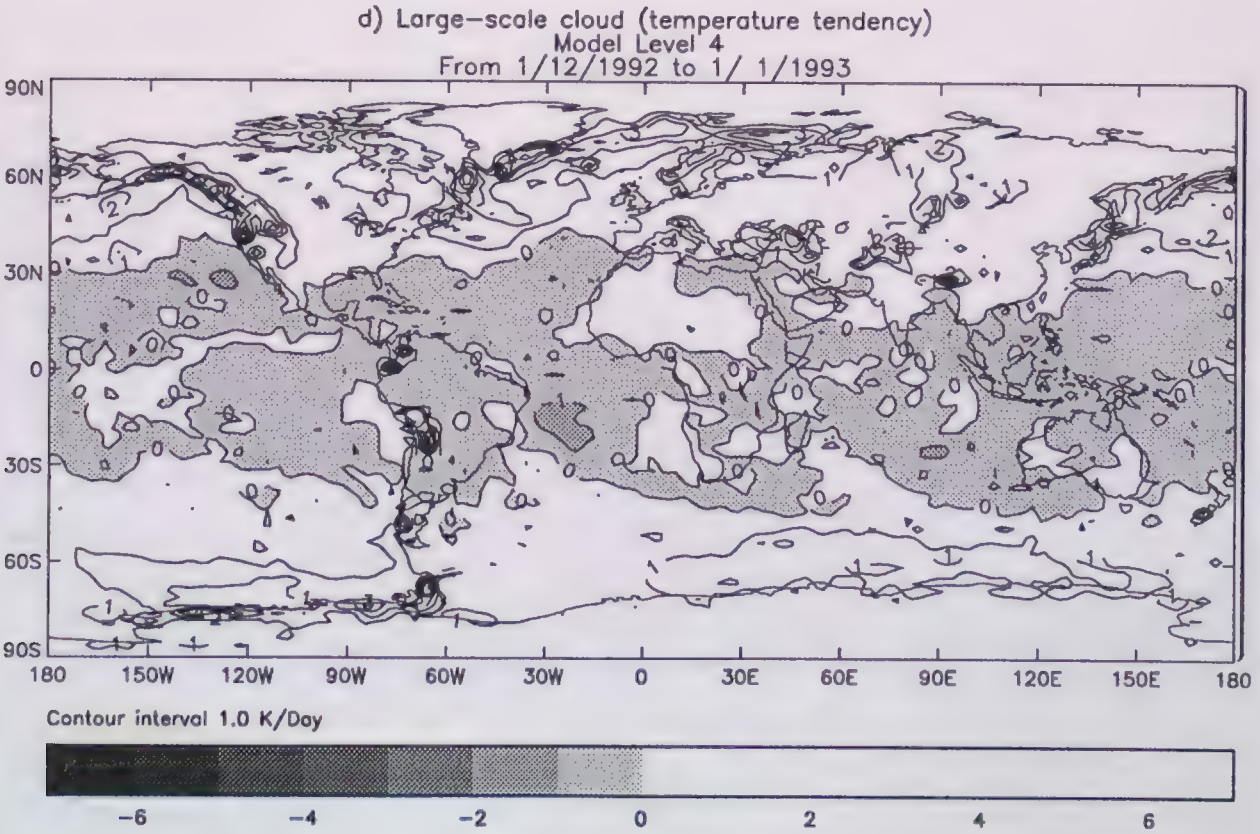

Figure 14 (continued)

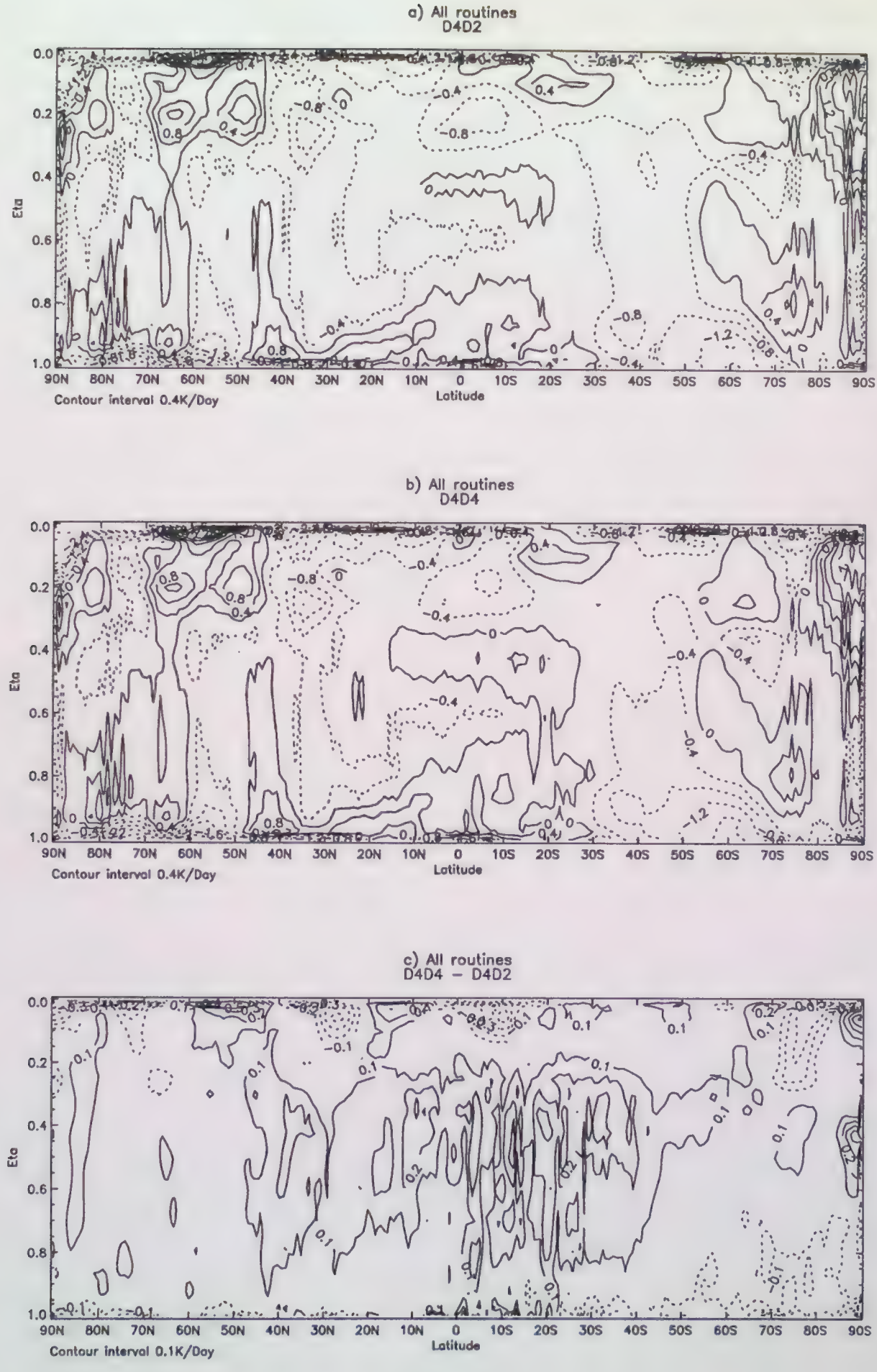
a) All routines
D4D2
Eta
Latitude
90N 80N 70N 60N 50N 40N 30N 20N 10N 0 10S 20S 30S 40S 50S 60S 70S 80S 90S
Contour interval 0.4K/Day
b) All routines
D4D4
Eta
Latitude
90N 80N 70N 60N 50N 40N 30N 20N 10N 0 10S 20S 30S 40S 50S 60S 70S 80S 90S
Contour interval 0.4K/Day
c) All routines
D4D4 – D4D2
Eta
Latitude
90N 80N 70N 60N 50N 40N 30N 20N 10N 0 10S 20S 30S 40S 50S 60S 70S 80S 90S
Contour interval 0.1K/Day

Figure 15

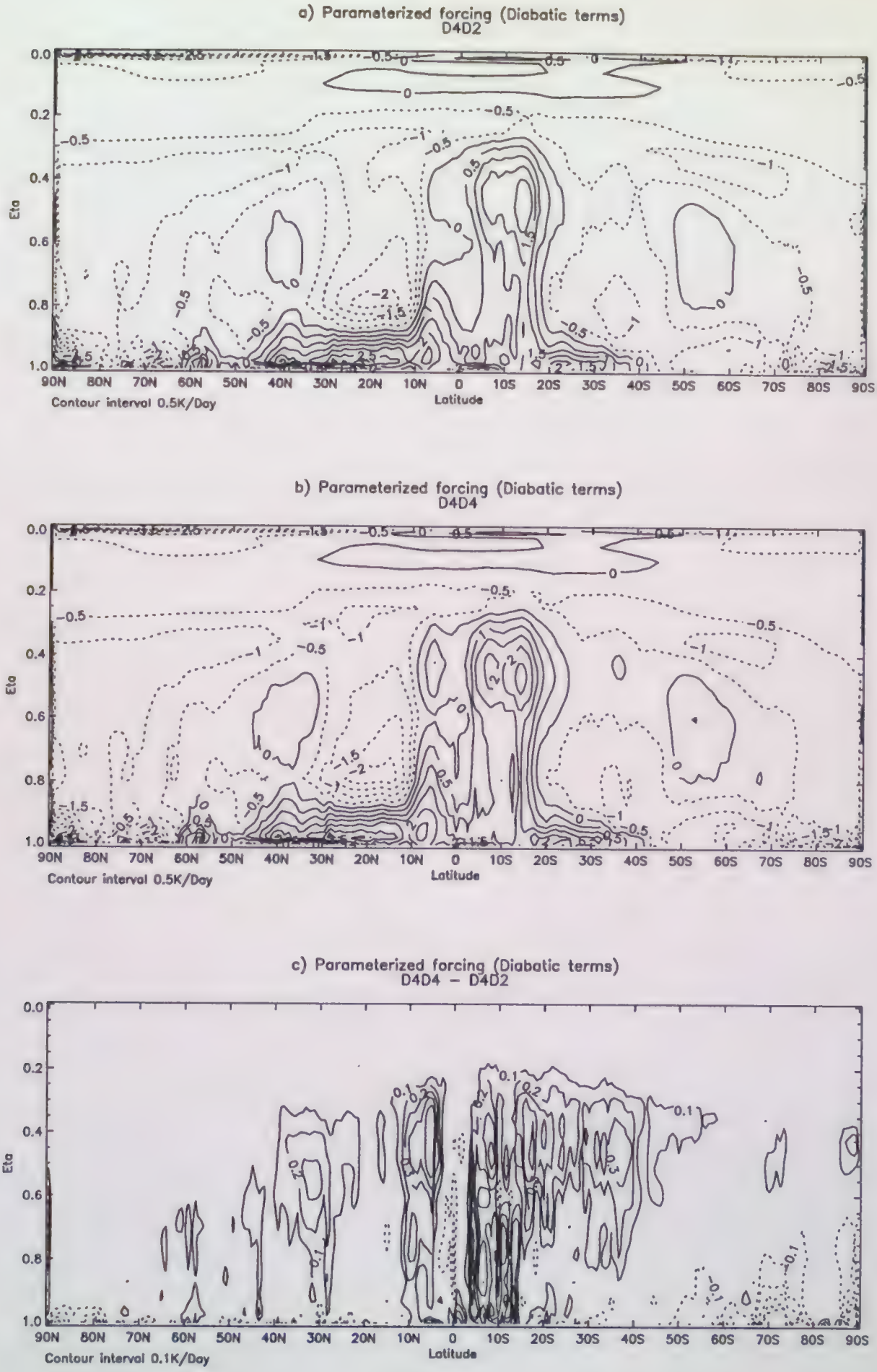
a) Parameterized forcing (Diabatic terms)
D4D2
Eta
Latitude
90N 80N 70N 60N 50N 40N 30N 20N 10N 0 10S 20S 30S 40S 50S 60S 70S 80S 90S
Contour interval 0.5K/Day
b) Parameterized forcing (Diabatic terms)
D4D4
Eta
Latitude
90N 80N 70N 60N 50N 40N 30N 20N 10N 0 10S 20S 30S 40S 50S 60S 70S 80S 90S
Contour interval 0.5K/Day
c) Parameterized forcing (Diabatic terms)
D4D4 – D4D2
Eta
Latitude
90N 80N 70N 60N 50N 40N 30N 20N 10N 0 10S 20S 30S 40S 50S 60S 70S 80S 90S
Contour interval 0.1K/Day

Figure 16

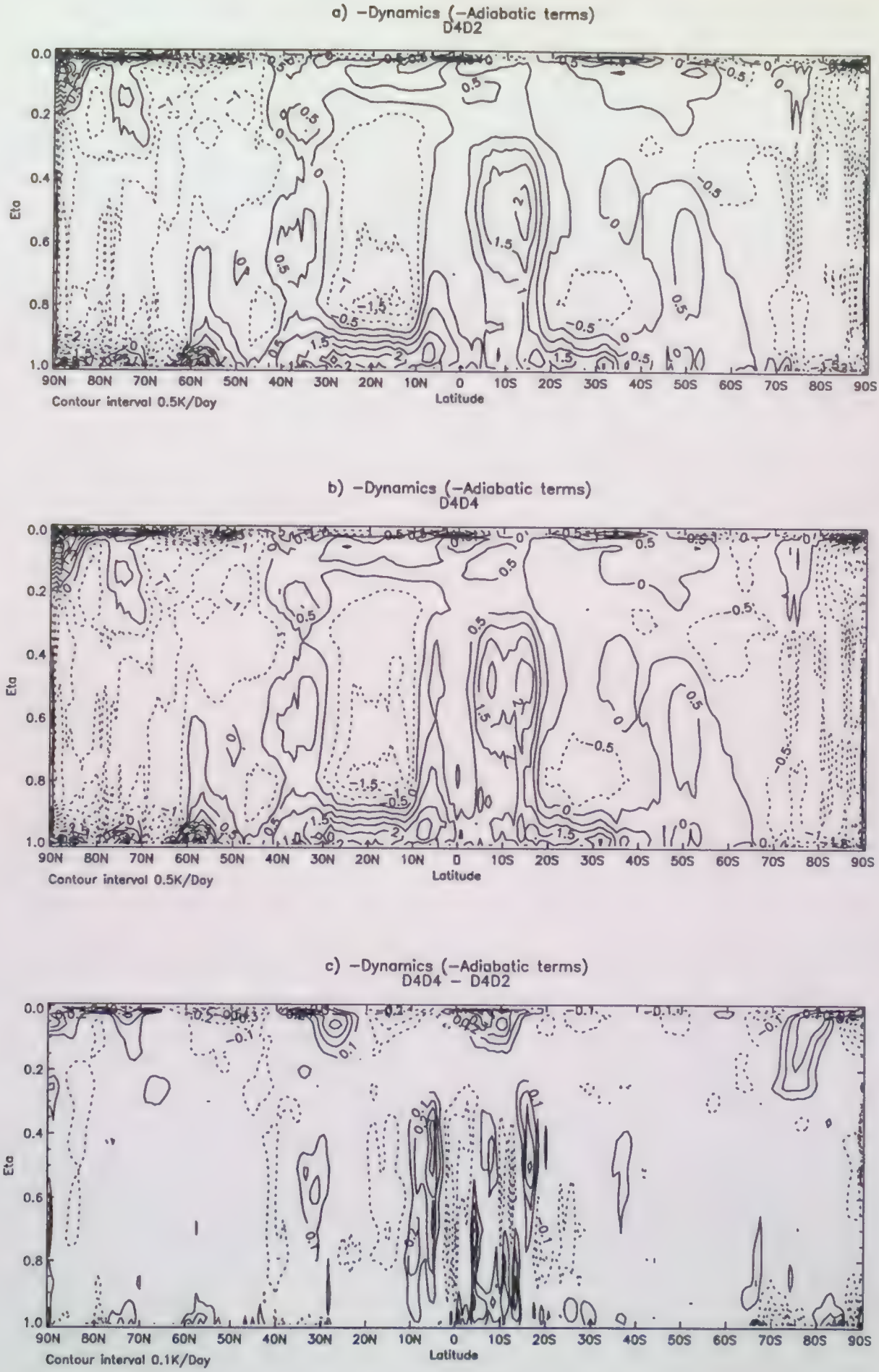
a) −Dynamics (−Adiabatic terms)
D4D2
Eta
Latitude
Contour interval 0.5K/Day
b) −Dynamics (−Adiabatic terms)
D4D4
Eta
Latitude
Contour interval 0.5K/Day
c) −Dynamics (−Adiabatic terms)
D4D4 − D4D2
Eta
Latitude
Contour interval 0.1K/Day

Figure 17

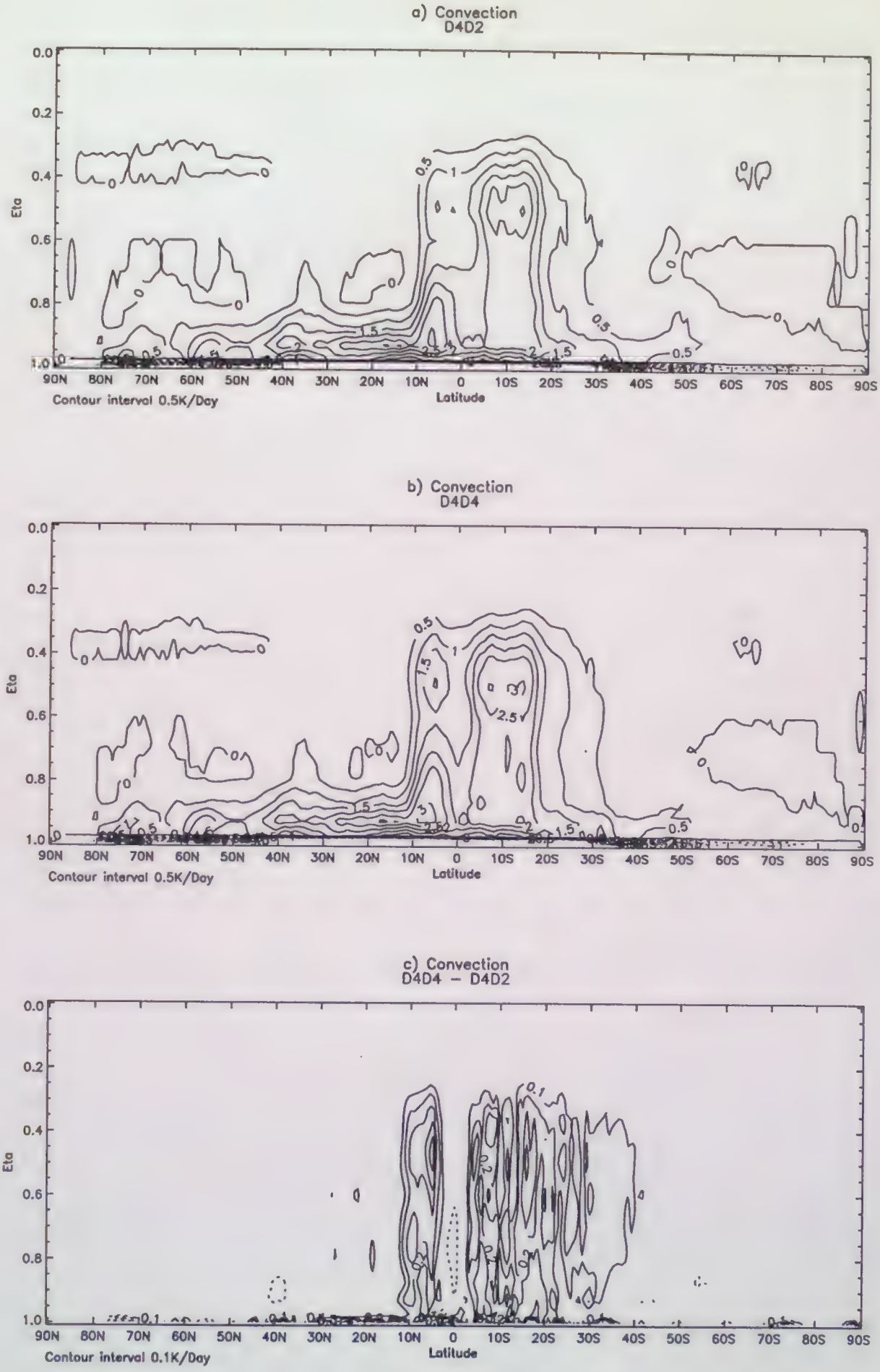
a) Convection
D4D2
Eta
0.0
0.2
0.4
0.6
0.8
1.0
90N 80N 70N 60N 50N 40N 30N 20N 10N 0 10S 20S 30S 40S 50S 60S 70S 80S 90S
Latitude
Contour interval 0.5K/Day
b) Convection
D4D4
Eta
0.0
0.2
0.4
0.6
0.8
1.0
90N 80N 70N 60N 50N 40N 30N 20N 10N 0 10S 20S 30S 40S 50S 60S 70S 80S 90S
Latitude
Contour interval 0.5K/Day
c) Convection
D4D4 – D4D2
Eta
0.0
0.2
0.4
0.6
0.8
1.0
90N 80N 70N 60N 50N 40N 30N 20N 10N 0 10S 20S 30S 40S 50S 60S 70S 80S 90S
Latitude
Contour interval 0.1K/Day

Figure 18

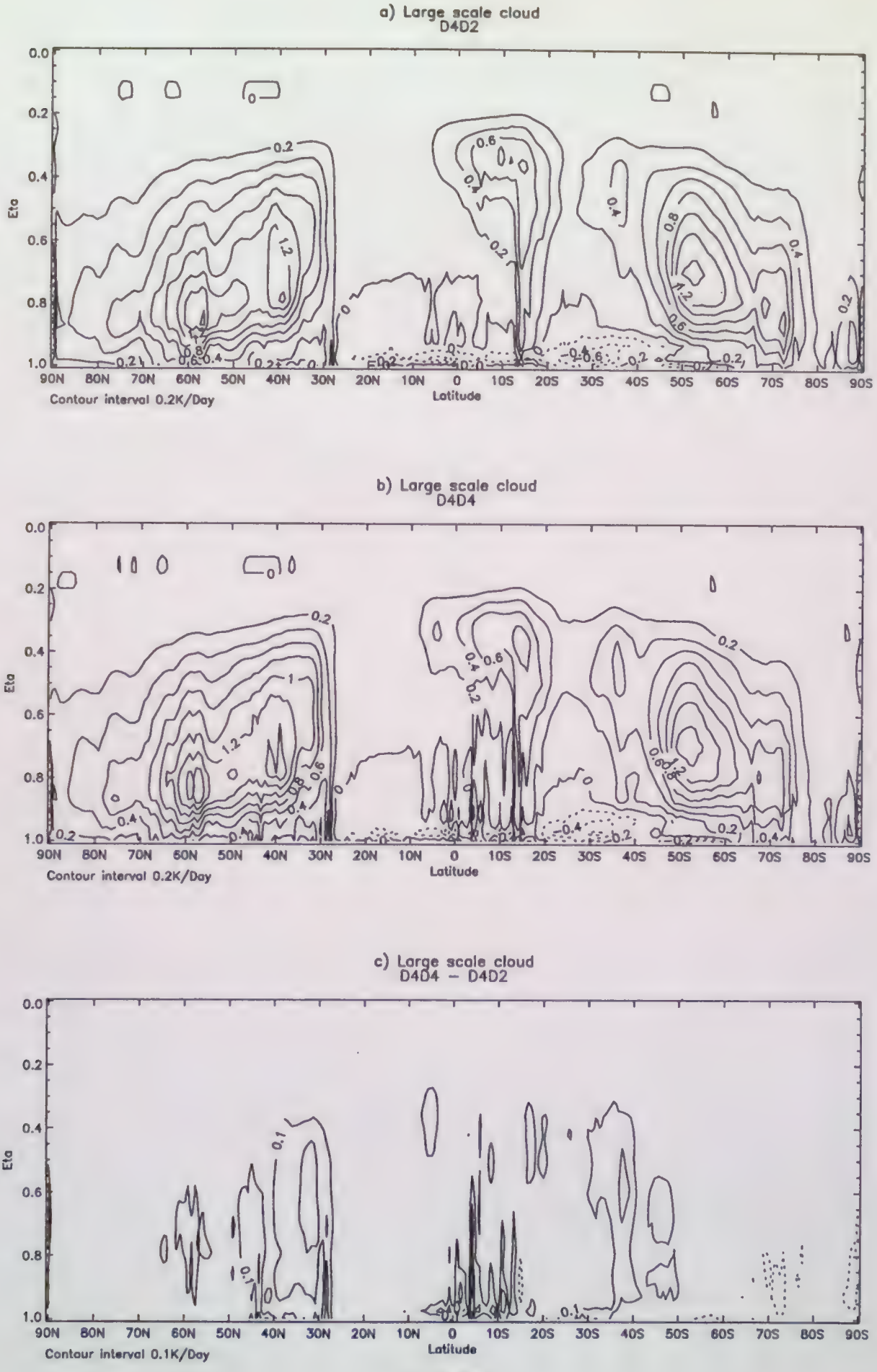
a) Large scale cloud
D4D2
Eta
Latitude
Contour interval 0.2K/Day
b) Large scale cloud
D4D4
Eta
Latitude
Contour interval 0.2K/Day
c) Large scale cloud
D4D4 – D4D2
Eta
Latitude
Contour interval 0.1K/Day

Figure 19

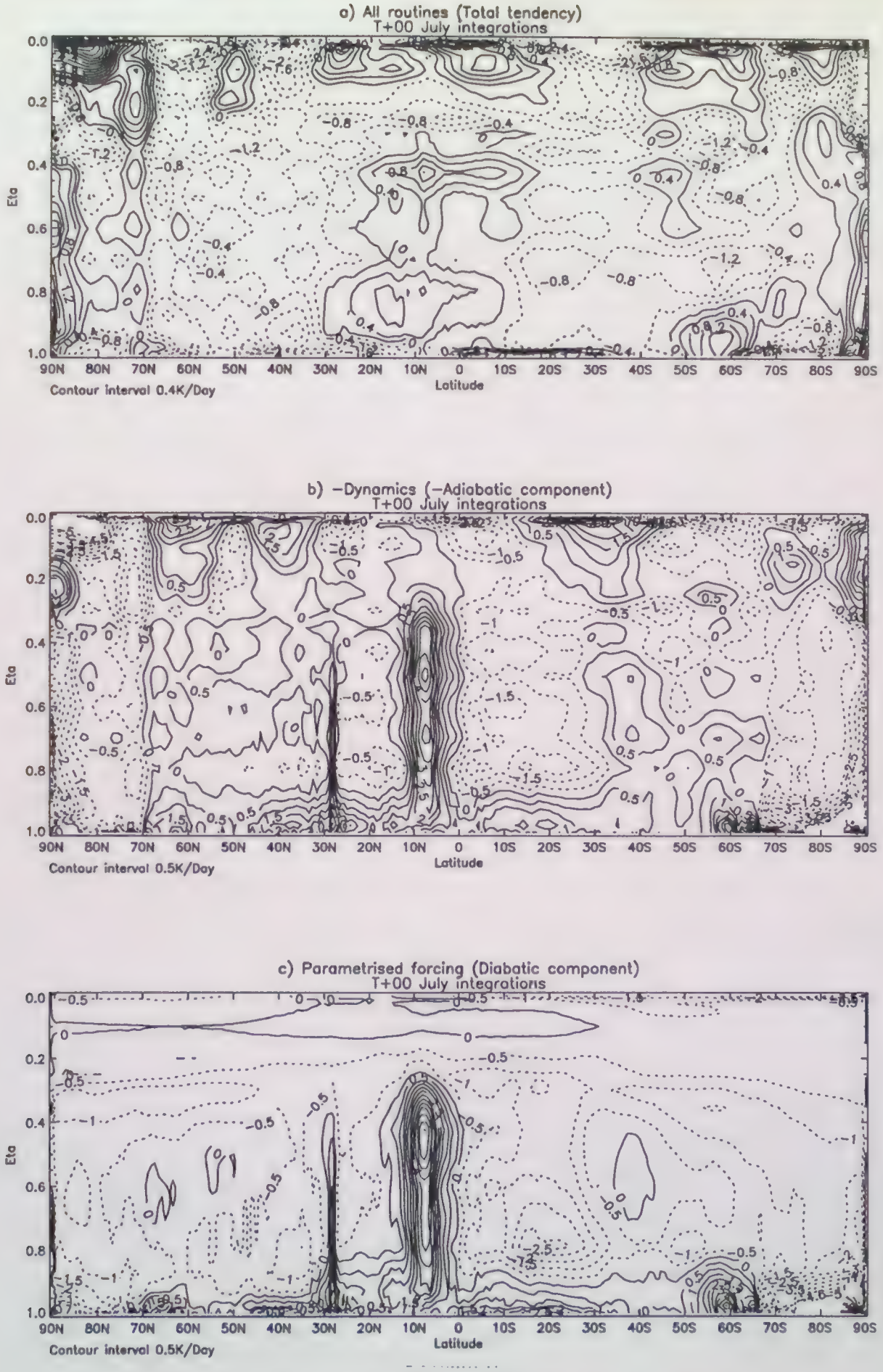
a) All routines (Total tendency)
T+00 July integrations
Eta
Latitude
Contour interval 0.4K/Day
b) −Dynamics (−Adiabatic component)
T+00 July integrations
Eta
Latitude
Contour interval 0.5K/Day
c) Parametrised forcing (Diabatic component)
T+00 July integrations
Eta
Latitude
Contour interval 0.5K/Day

Figure 20

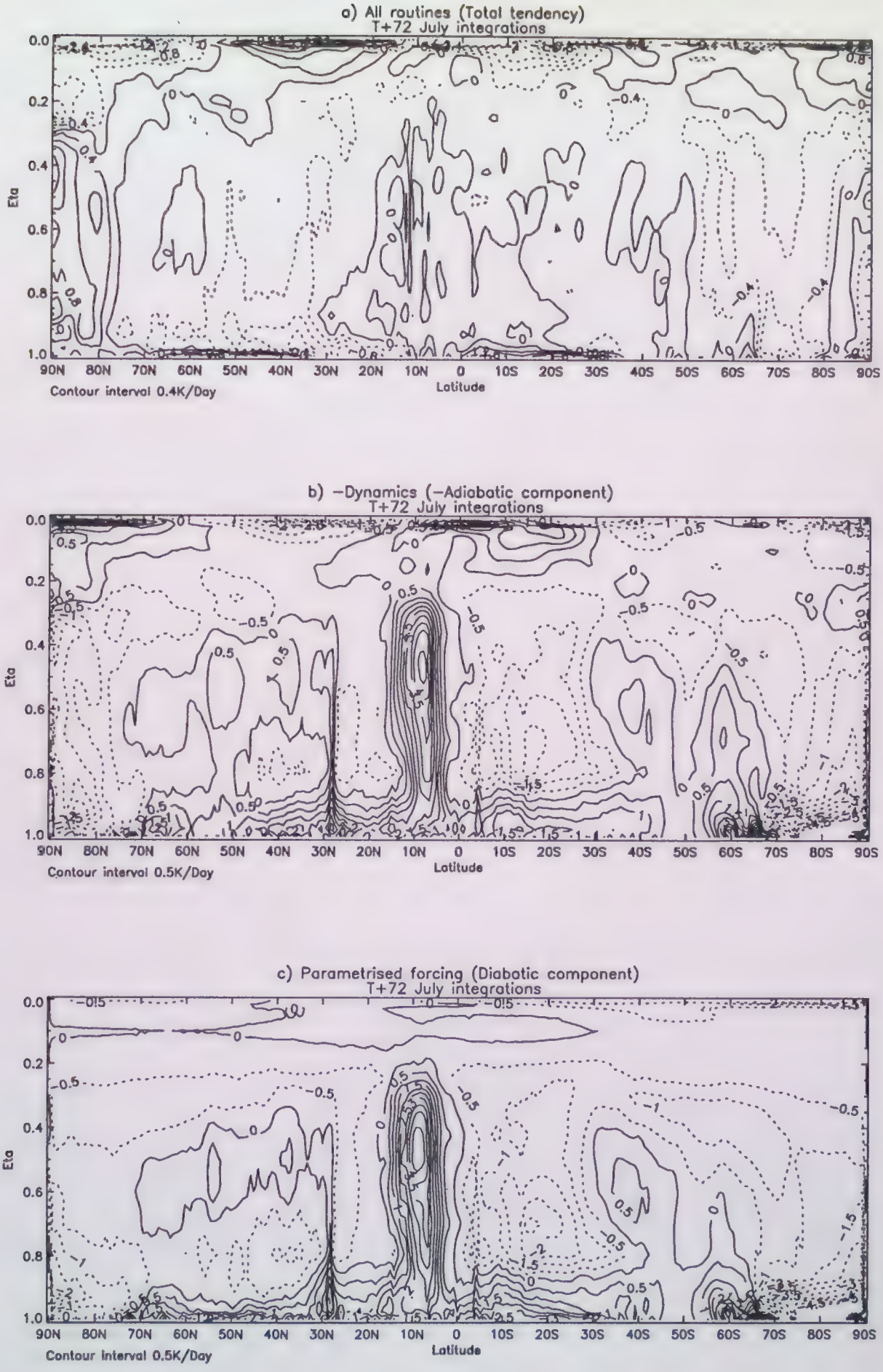
a) All routines (Total tendency)
T+72 July integrations
Eta
Latitude
Contour interval 0.4K/Day
b) −Dynamics (−Adiabatic component)
T+72 July integrations
Eta
Latitude
Contour interval 0.5K/Day
c) Parametrised forcing (Diabatic component)
T+72 July integrations
Eta
Latitude
Contour interval 0.5K/Day

Figure 21

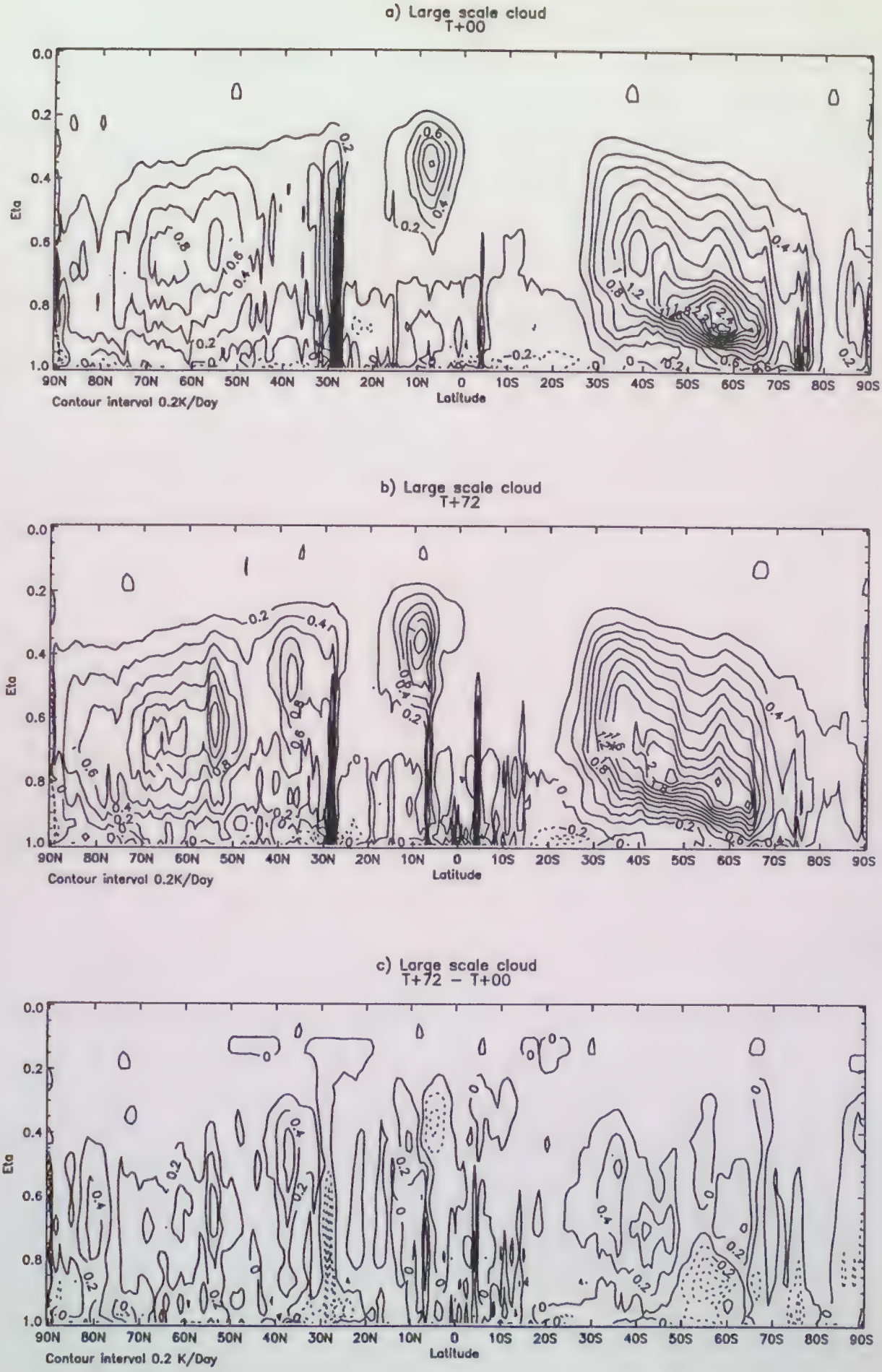
a) Large scale cloud
T+00
Eta
Latitude
Contour interval 0.2K/Day
b) Large scale cloud
T+72
Eta
Latitude
Contour interval 0.2K/Day
c) Large scale cloud
T+72 – T+00
Eta
Latitude
Contour interval 0.2 K/Day

Figure 22

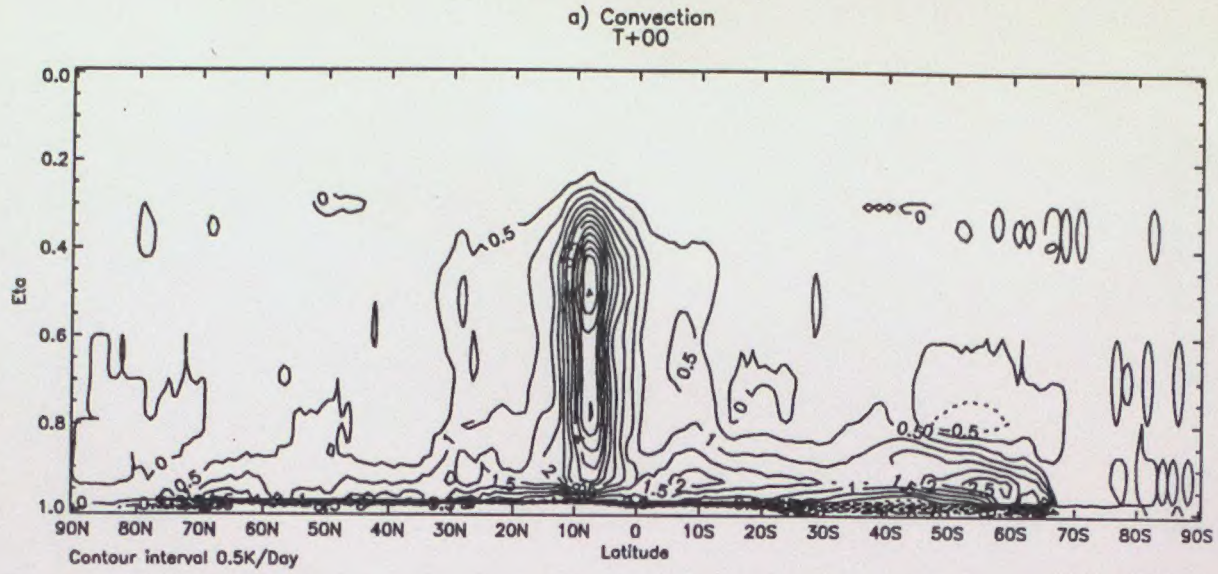
a) Convection
T+00
Eta
0.0
0.2
0.4
0.6
0.8
1.0
90N 80N 70N 60N 50N 40N 30N 20N 10N 0 10S 20S 30S 40S 50S 60S 70S 80S 90S
Latitude
Contour interval 0.5K/Day

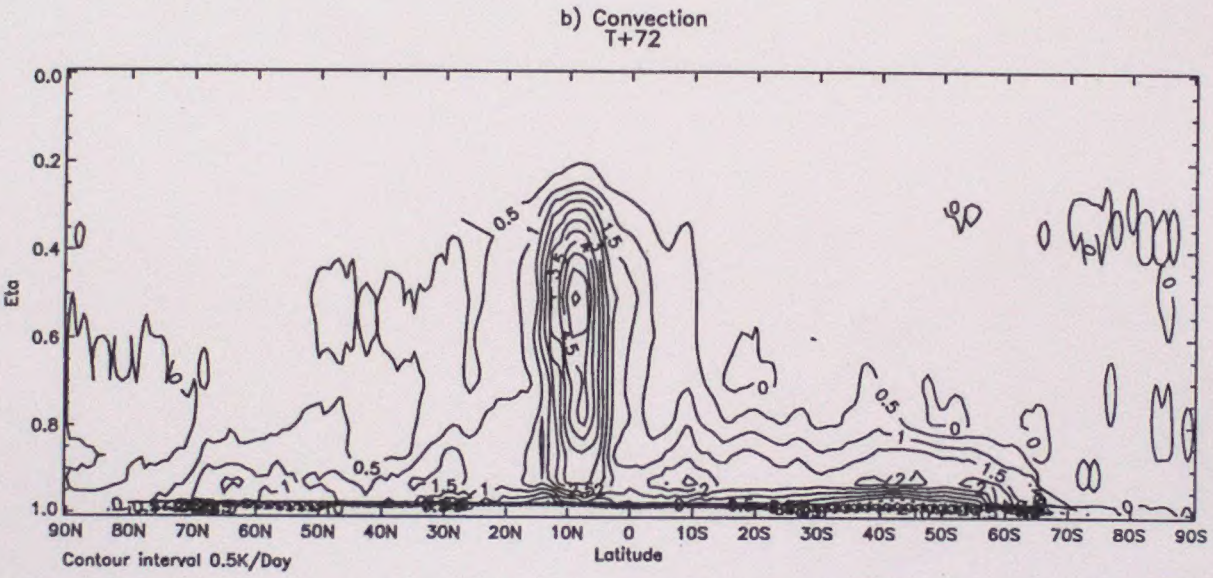
b) Convection
T+72
Eta
0.0
0.2
0.4
0.6
0.8
1.0
90N 80N 70N 60N 50N 40N 30N 20N 10N 0 10S 20S 30S 40S 50S 60S 70S 80S 90S
Latitude
Contour interval 0.5K/Day

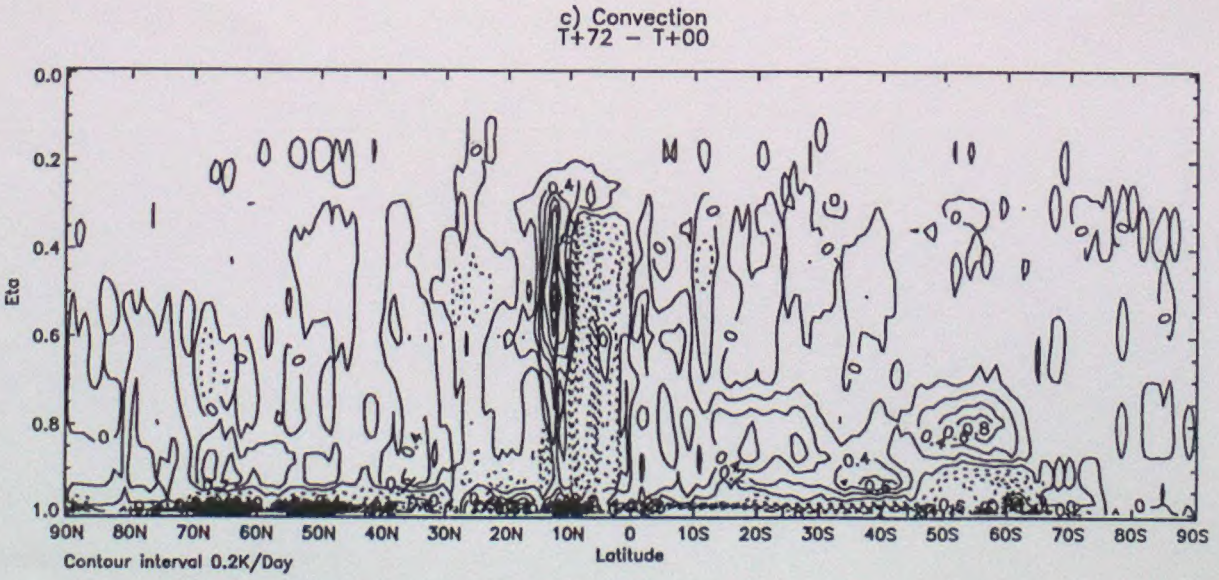
c) Convection
T+72 – T+00
Eta
0.0
0.2
0.4
0.6
0.8
1.0
90N 80N 70N 60N 50N 40N 30N 20N 10N 0 10S 20S 30S 40S 50S 60S 70S 80S 90S
Latitude
Contour interval 0.2K/Day

Figure 23

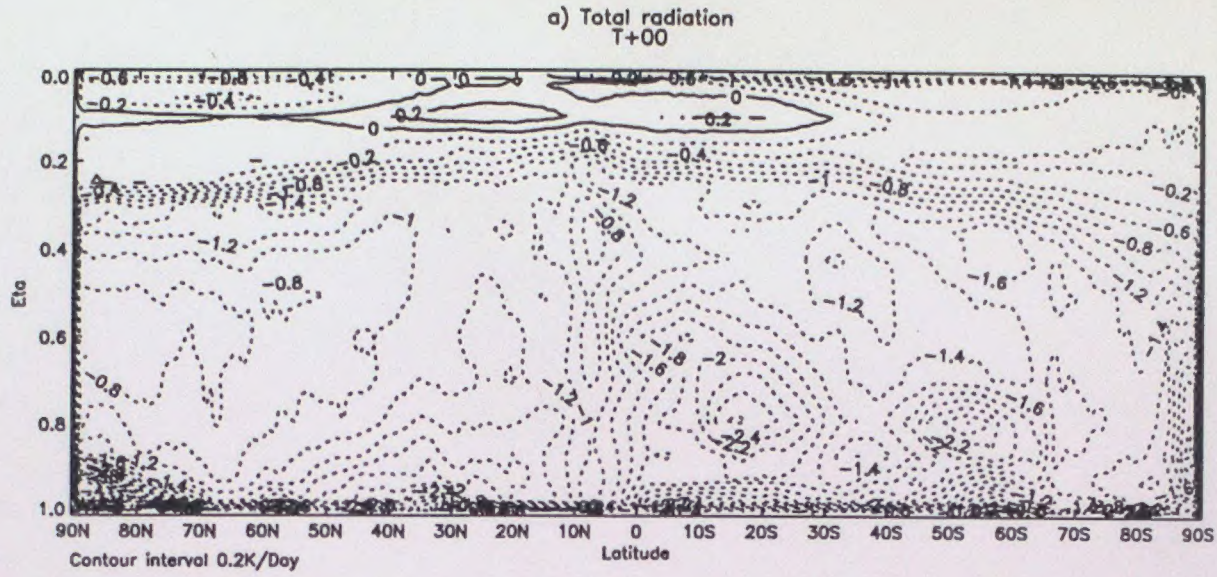
a) Total radiation
T+00
Eta
Latitude
90N 80N 70N 60N 50N 40N 30N 20N 10N 0 10S 20S 30S 40S 50S 60S 70S 80S 90S
Contour interval 0.2K/Day

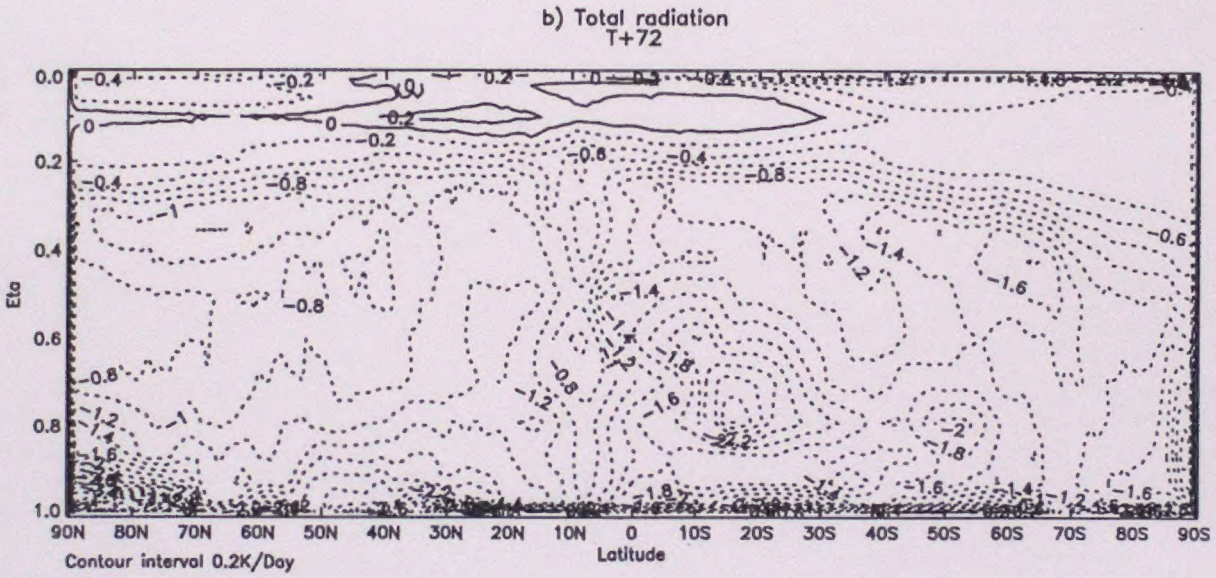
b) Total radiation
T+72
Eta
Latitude
90N 80N 70N 60N 50N 40N 30N 20N 10N 0 10S 20S 30S 40S 50S 60S 70S 80S 90S
Contour interval 0.2K/Day

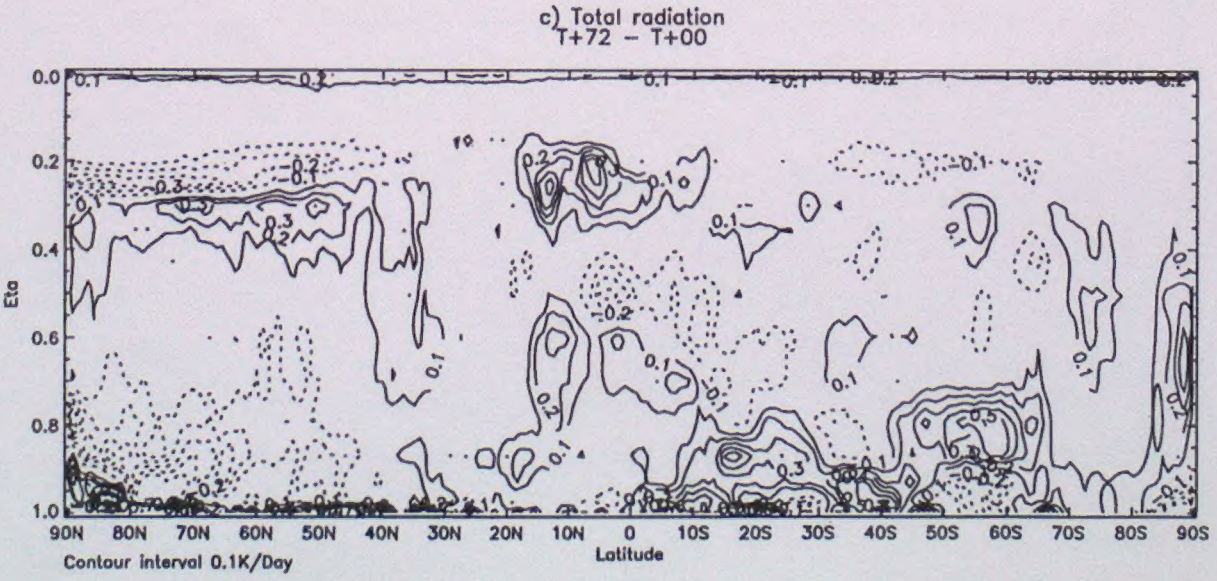
c) Total radiation
T+72 - T+00
Eta
Latitude
90N 80N 70N 60N 50N 40N 30N 20N 10N 0 10S 20S 30S 40S 50S 60S 70S 80S 90S
Contour interval 0.1K/Day

Figure 24

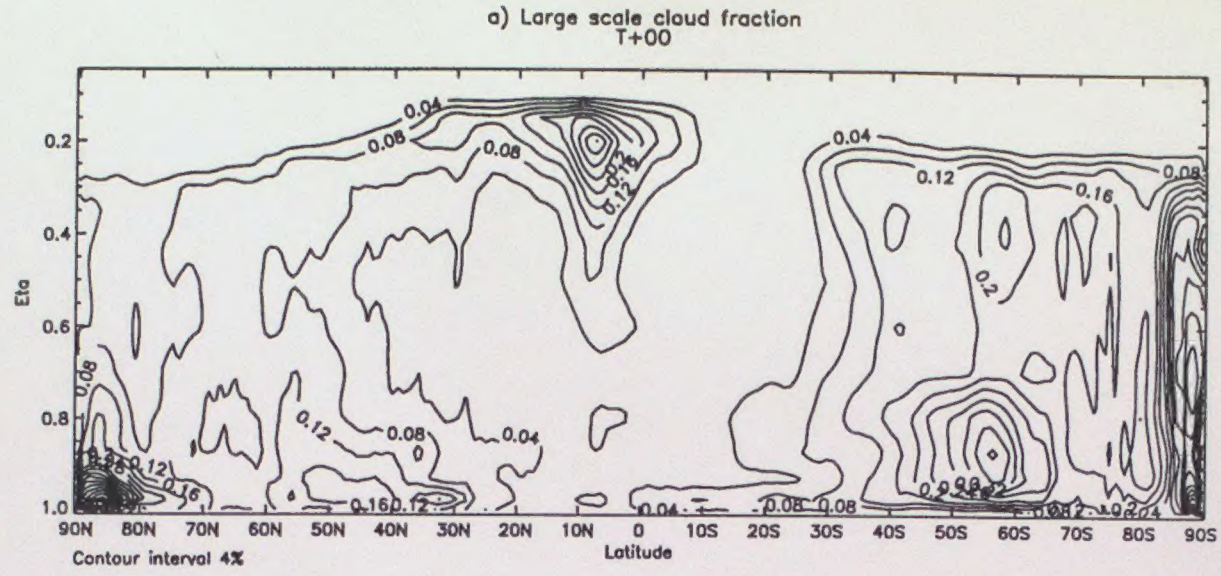
a) Large scale cloud fraction
T+00
Eta
Latitude
90N 80N 70N 60N 50N 40N 30N 20N 10N 0 10S 20S 30S 40S 50S 60S 70S 80S 90S
Contour interval 4%

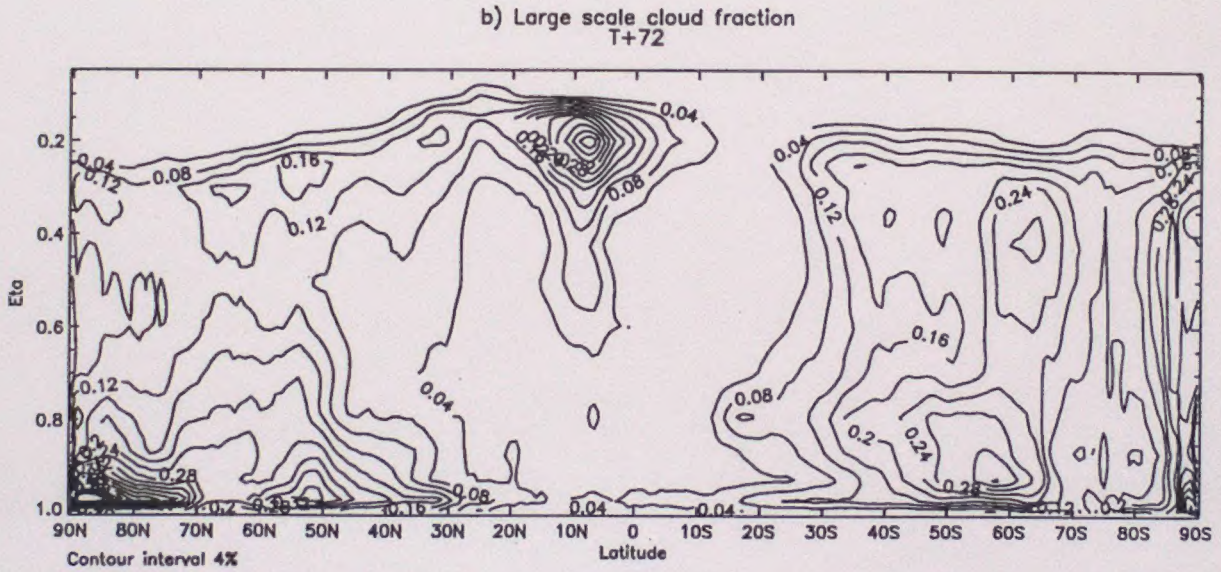
b) Large scale cloud fraction
T+72
Eta
Latitude
90N 80N 70N 60N 50N 40N 30N 20N 10N 0 10S 20S 30S 40S 50S 60S 70S 80S 90S
Contour interval 4%

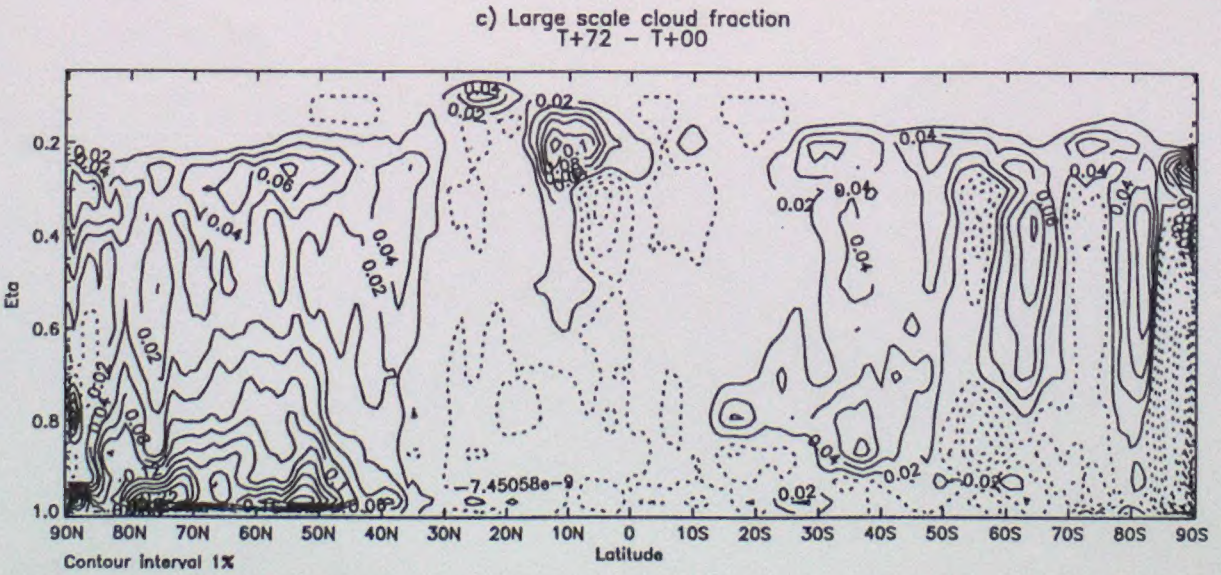
c) Large scale cloud fraction
T+72 – T+00
Eta
-7.45058e-9
Latitude
90N 80N 70N 60N 50N 40N 30N 20N 10N 0 10S 20S 30S 40S 50S 60S 70S 80S 90S
Contour interval 1%

Figure 25

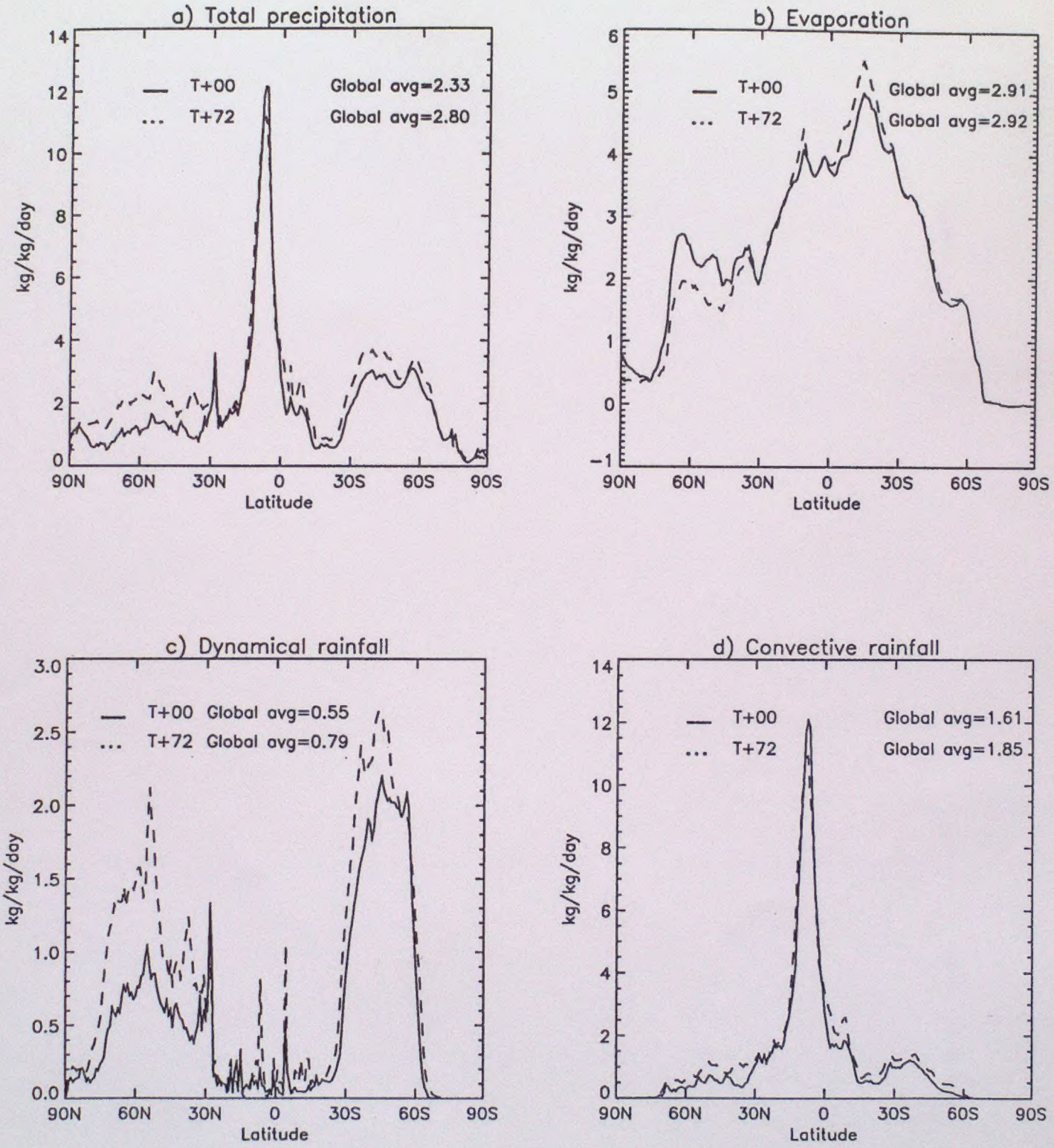
a) Total precipitation
T+00
T+72
Global avg=2.33
Global avg=2.80
kg/kg/day
Latitude
90N
60N
30N
0
30S
60S
90S
b) Evaporation
Global avg=2.91
Global avg=2.92
c) Dynamical rainfall
T+00 Global avg=0.55
T+72 Global avg=0.79
d) Convective rainfall
Global avg=1.61
Global avg=1.85

Figure 26